INTERNATIONAL JOURNAL OF
NUMERICAL ANALYSIS AND MODELING
Volume x, Number 0xx, Pages 1–18



# HYBRID STRESS FINITE VOLUME METHOD FOR LINEAR ELASTICITY PROBLEMS

YONGKE WU, XIAOPING XIE, AND LONG CHEN

**Abstract.** A hybrid stress finite volume method is proposed for linear elasticity equations. In this new method, a finite volume formulation is used for the equilibrium equation, and a hybrid stress quadrilateral finite element discretization, with continuous piecewise isoparametric bilinear displacement interpolation and two types of stress approximation modes, is used for the constitutive equation. The method is shown to be free from Poisson-locking and of first order convergence. Numerical experiments confirm the theoretical results.

**Key words.** finite volume method, hybrid stress method, quadrilateral element, Poisson-locking.

## 1. Introduction

The Finite Volume Method (FVM) is a popular class of discretization techniques for partial differential equations. One main reason for its increasing popularity is that FVM combines the geometric flexibility of the Finite Element Method (FEM) with the local conservation of physical quantities; see [27] for more interesting properties of FVM. By these virtues, FVM has been extensively used in the fields of Computational Fluid Dynamics (CFD), heat and mass transfer (see, eg [20, 22, 25, 30, 41, 44]).

In the context of Computational Solid Mechanics (CSM), however, the use of FVM has not been further explored, whereas FEM plays the dominate role because of its runaway success. Recently to simulate of multiphysical problems using flow, solid mechanics, electromagnetic, heat transfer, etc. in a coupled manner, there is increasing demand to discretize the solid mechanics using FVM [17].

Wilkins [47] made an early attempt of using FVM concept in CSM by using an alternative approximation to derivatives in a cell. Oñate, Cervera, and Zienkiewicz [29] showed that FVM could be considered to be a particular case of FEM with a non-Galerkin weighting. In recent years, there has been much effort in the development and numerical investigation of FVM in CSM (see, eg [6, 9, 18, 19, 24, 40, 46]).

In this paper, we shall construct a coupling method of FVM and the hybrid stress FEM [32, 36, 50] for linear elasticity problems and present a complete numerical analysis for *a priori* error estimates. The idea follows from Wapperom and Webster [45], where FEM and FVM was coupled to simulate viscoelastic flows, and from Chen [12], where a class of high order finite volume methods was developed for second order elliptic equations by combining high order finite element methods and a linear finite volume method. We use hybrid stress FEM for the constitutive equation, and FVM for the equilibrium equation by introducing piecewise constant test functions in a dual mesh. We choose PS-stress

Received by the editors January x, xxxx and, in revised form, x xx, xxxx.
2000 *Mathematics Subject Classification.* 35R35, 49J40, 60G40.

mode [32] or ECQ4-mode [50] to approximate the stress tensor, and use isoparametric bilinear element to approximate the displacement. By doing so, our new method can inherit some virtues of hybrid stress FEM, e.g. the robustness with respect to Poisson locking. Meanwhile, the equilibrium equation holds locally (on every control volume). Note that the governing equations for solid body and fluid mechanics are the same but only differ in constitutive relations. Our method can be readily used to simulate the coupling of fluid flows and solid body deformation.

We shall analyze our new method following the mixed FEM theory [8, 10]. To the authors best knowledge, there are only handful rigorous analysis of mixed FVM on general quadrilateral meshes for elliptic equations [13, 14, 15, 16] and no such results for linear elasticity. Our discretization will result in a generalized saddle point system in the form

$$\begin{pmatrix} \mathcal{A} & \mathcal{B}^T \\ \mathcal{C} & 0 \end{pmatrix} \begin{pmatrix} \boldsymbol{\sigma} \\ \boldsymbol{u} \end{pmatrix} = \begin{pmatrix} 0 \\ \boldsymbol{f} \end{pmatrix}. \tag{1}$$

The analysis of the saddle point system (1) is much more involved than the symmetric case $\mathcal{B} = \mathcal{C}$. In addition to the verification of the inf-sup condition for operators $\mathcal{B}$ and $\mathcal{C}$, we need to prove that their kernels match: $\dim(\ker(\mathcal{B})) = \dim(\ker(\mathcal{C}))$ and a inf-sup condition of $\mathcal{A}$ on these two null spaces [8, 10]. Fast solvers for the non-symmetric saddle point system (1) is also more difficult than the symmetric case.

We shall overcome these difficulties by a perturbation of $\mathcal{B}$ to $\tilde{\mathcal{B}}$ using the technique developed in [54]. We show that $\tilde{\mathcal{B}} = \mathcal{D}\mathcal{C}$ with a symmetric and positive definite matrix $\mathcal{D}$. Therefore $\ker(\tilde{\mathcal{B}}) = \ker(\mathcal{C})$ and furthermore, by a scaling, (1) becomes symmetric. Note that although our system is in the mixed form, the stress unknowns can be eliminated element-wise and the resulting Schur complement is symmetric and positive definite (SPD). We can then solve this SPD system efficiently by using multigrid solvers or preconditioned conjugate gradient method with multilevel preconditioners.

In this paper, we use notation $a \lesssim b$ (or $a \gtrsim b$) to represent that there exists a constant $C$ independent of mesh size $h$ and the Lamé constant $\lambda$ such that $a \leq Cb$ (or $a \geq Cb$), and use $a \eqsim b$ to denote $a \lesssim b \lesssim a$.

The rest of this paper is organized as follows. In section 2, we describe the model problem, introduce the isoparametric bilinear element, and review the hybrid stress FEM. Section 3 defines our hybrid stress finite volume method based on PS or ECQ4 stress mode. Section 4 presents stability analysis. Section 5 derives *a priori* error estimates. In the final section, we give some numerical results in support of theoretical ones.

## 2. Preliminary

In this section, we present the model problem and introduce isoparametric elements and hybrid finite element methods.

**2.1. A model problem.** Let $\Omega \subset \mathbb{R}^2$ be a bounded polygonal domain with boundary $\Gamma = \Gamma_D \cup \Gamma_N$, where meas$(\Gamma_D) > 0$. We consider the following linear elasticity problem

$$\left\{\begin{array}{rlcll} -\text{div} & \boldsymbol{\sigma} & = & \boldsymbol{f} & \text{in } \Omega, \\ & \boldsymbol{\sigma} & = & \mathbb{C}\epsilon(\boldsymbol{u}) & \text{in } \Omega, \\ & \boldsymbol{u} & = & 0 & \text{on } \Gamma_D, \\ & \boldsymbol{\sigma}\boldsymbol{n} & = & \boldsymbol{g}, & \text{on } \Gamma_N \end{array}\right. \tag{2}$$

where $\boldsymbol{\sigma} \in \mathbb{R}^{2\times 2}_{\text{sym}}$ denotes the symmetric stress tensor field, $\boldsymbol{u} = (u, v)^T \in \mathbb{R}^2$ the displacement field, $\epsilon(\boldsymbol{u}) = \frac{1}{2}(\nabla \boldsymbol{u} + (\nabla \boldsymbol{u})^T)$ the strain tensor, $\boldsymbol{f} \in \mathbb{R}^2$ the body loading density, $\boldsymbol{g} \in \mathbb{R}^2$ the surface traction, $\boldsymbol{n}$ the unit outward vector norm to $\Gamma_N$, and $\mathbb{C}$ the elasticity module tensor with

$$\mathbb{C}\epsilon(\boldsymbol{u}) = 2\mu\epsilon(\boldsymbol{u}) + \lambda \text{div}\boldsymbol{u}\, \boldsymbol{I}, \qquad \mathbb{C}^{-1}\boldsymbol{\sigma} = \frac{1}{2\mu}\left(\boldsymbol{\sigma} - \frac{\lambda}{2(\mu+\lambda)}\text{tr}(\boldsymbol{\sigma})\, \boldsymbol{I}\right). \tag{3}$$

Here $\boldsymbol{I}$ is the $2\times 2$ identity tensor, $\text{tr}(\boldsymbol{\sigma})$ the trace of the stress tensor $\boldsymbol{\sigma}$, and $\mu$, $\lambda$ the Lamé parameters given by $\mu = \dfrac{E}{2(1+\nu)}$, $\lambda = \dfrac{E\nu}{(1+\nu)(1-2\nu)}$ for plane strain problems, and by $\mu = \dfrac{E}{2(1+\nu)}$, $\lambda = \dfrac{E\nu}{(1+\nu)(1-\nu)}$ for plane stress problems, with $0 < \nu < 0.5$ the Poisson ratio and $E$ the Young's modulus.

The weak formulation of (2) is: Find $(\boldsymbol{\sigma}, \boldsymbol{u}) \in L^2(\Omega; \mathbb{R}^{2\times 2}_{sym}) \times (H^1_{0,D})^2$ such that

$$\left\{\begin{array}{ll} \displaystyle\int_\Omega \epsilon(\boldsymbol{u}) : \boldsymbol{\tau} \mathrm{d}x\mathrm{d}y = \int_\Omega \mathbb{C}^{-1}\boldsymbol{\sigma} : \boldsymbol{\tau} \mathrm{d}x\mathrm{d}y & \text{for all } \boldsymbol{\tau} \in L^2(\Omega; \mathbb{R}^{2\times 2}_{sym}) \\ \displaystyle\int_\Omega \boldsymbol{\sigma} : \epsilon(\boldsymbol{v}) \mathrm{d}x\mathrm{d}y = \int_\Omega \boldsymbol{f}\cdot\boldsymbol{v}\mathrm{d}x\mathrm{d}y + \int_{\Gamma_N} \boldsymbol{g}\cdot\boldsymbol{v}\mathrm{d}s & \text{for all } \boldsymbol{v} \in (H^1_{0,D})^2. \end{array}\right. \tag{4}$$

where $L^2(\Omega; \mathbb{R}^{2\times 2}_{sym})$ denotes the space of square-integrable symmetric tensors, $(H^1_{0,D})^2 = \{\boldsymbol{v} \in (H^1(\Omega))^2 : \ \boldsymbol{v}|_{\Gamma_D} = 0\}$. The existence and uniqueness of the weak solution to (4) can be found in [52].

We shall consider a coupling method of FVM and FEM for equations (2). The Neumann type boundary condition can be build into the weak formulation. For simplicity of exposition, we consider only the case $\Gamma_N = \emptyset$. Note that in this case it holds the compatibility condition $\int_\Omega \text{tr}(\boldsymbol{\sigma}) = 0$.

In this paper, we will use $\|\cdot\|_k$ and $|\cdot|_k$ to denote $H^k$ norm and semi-norm for both vectors and tensors. And use $\|\cdot\|$ to denote $L^2$ norm for both vectors and tensors.

**2.2. Isoparametric transformation.** Let $\{\mathcal{T}_h\}_{h>0}$ be conventional quadrilateral meshes of $\Omega$. Let $h_K$ denote the diameter of quadrilateral $K \in \mathcal{T}_h$, and $h = \max\limits_{K\in\mathcal{T}_h} h_K$. Let $Z_i(x_i, y_i)$, $1 \le i \le 4$ be four vertices of $K$, and $T_i$ the sub-triangle of $K$ with vertices $Z_{i-1}$, $Z_i$ and $Z_{i+1}$ (the index on $Z_i$ is modulo four). Define

$$\rho_K = \min_{1\le i\le 4}\{ \text{ maximal radius of circles inscribed in } T_i\}.$$

Throughout this paper, we assume that $\{\mathcal{T}_h\}_{h>0}$ satisfy the following shape regular hypothesis: There exits a constant $\varrho > 2$ independent of $h$ such that for all $h > 0$ and $K \in \mathcal{T}_h$,

$$h_K \leq \varrho \rho_K. \tag{5}$$

We introduce two mesh conditions proposed by Shi [37].

**Condition (A).** The distance $d_K$ between the midpoints of the diagonals of any $K \in \mathcal{T}_h$ is of order $o(h_K)$ for all elements $K \in \mathcal{T}_h$ as $h \to 0$.

**Condition (B).** The distance $d_K$ between the midpoints of the diagonals of any $K \in \mathcal{T}_h$ is of order $O(h_K^2)$ for all elements $K \in \mathcal{T}_h$ as $h \to 0$.

The weaker condition (A) will be used in the analysis of stability and the stronger one (B) is used in the optimal order of convergence (see Sections 4-5 for details).

All quadrilaterals produced by a bi-section scheme of mesh subdivisions satisfy the stronger condition (B), i.e., $d_K = O(h_K^2)$ [37].

Let $\hat{K} = [-1, 1] \times [-1, 1]$ be the reference element with vertices $\hat{Z}_i$, $1 \leq i \leq 4$. There exits a unique invertible bilinear mapping $F_K$ that maps $\hat{K}$ onto $K$ with $F_K(\hat{Z}_i) = Z_i$, $1 \leq i \leq 4$ (Figure 1). The mapping $F_K$ is given by

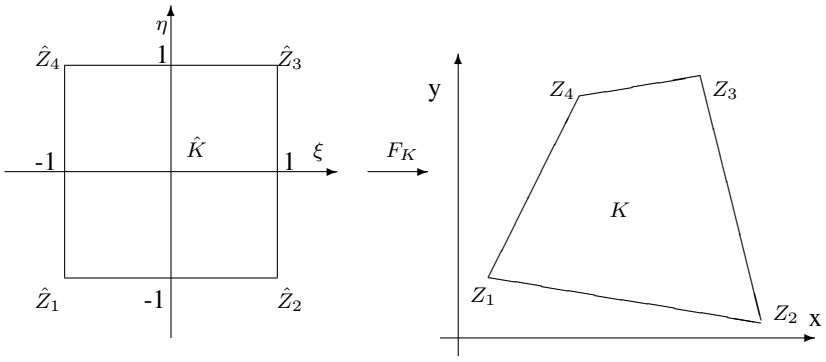


FIGURE 1. Bilinear transformation $F_K$ maps a reference element $\hat{K}$ (in the left) to the element $K$ (in the right).

$$\begin{pmatrix} x \\ y \end{pmatrix} = F_K(\xi, \eta) = \begin{pmatrix} a_0 + a_1\xi + a_2\eta + a_{12}\xi\eta \\ b_0 + b_1\xi + b_2\eta + b_{12}\xi\eta \end{pmatrix}, \tag{6}$$

where $(x, y) \in K$, $(\xi, \eta) \in \hat{K}$, and

$$\begin{pmatrix} a_0 & b_0 \\ a_1 & b_1 \\ a_2 & b_2 \\ a_{12} & b_{12} \end{pmatrix} = \frac{1}{4} \begin{pmatrix} 1 & 1 & 1 & 1 \\ -1 & 1 & 1 & -1 \\ -1 & -1 & 1 & 1 \\ 1 & -1 & 1 & -1 \end{pmatrix} \begin{pmatrix} x_1 & y_1 \\ x_2 & y_2 \\ x_3 & y_3 \\ x_4 & y_4 \end{pmatrix}.$$

**Remark 2.1.** By the choice of the ordering of vertices (Figure 1), we always have $a_1 > 0$, $b_2 > 0$. Let $O_1$ and $O_2$ be mid-points of two diagonals of $K \in \mathcal{T}_h$. Note that vector $\overrightarrow{O_1O_2} = -2\langle a_{12}, b_{12}\rangle$ and therefore $a_{12}^2 + b_{12}^2 = 4d_K^2$. Under condition (A) or condition (B), $|a_{12}|$ and $|b_{12}|$ are high order terms of $h_K$. Especially when $K$ is a parallelogram, it holds $a_{12} = b_{12} = 0$, and $F_K$ is reduced to an affine mapping. □

The Jacobi matrix of the transformation $F_K$ is

$$DF_K(\xi,\eta) = \begin{pmatrix} \frac{\partial x}{\partial \xi} & \frac{\partial x}{\partial \eta} \\ \frac{\partial y}{\partial \xi} & \frac{\partial y}{\partial \eta} \end{pmatrix} = \begin{pmatrix} a_1 + a_{12}\eta & a_2 + a_{12}\xi \\ b_1 + b_{12}\eta & b_2 + b_{12}\xi \end{pmatrix},$$

and the Jacobian of $F_K$ is

$$J_K(\xi,\eta) = \det(DF_K) = J_0 + J_1\xi + J_2\eta,$$

with $J_0 = a_1b_2 - a_2b_1,\ J_1 = a_1b_{12} - a_{12}b_1,\ J_2 = a_{12}b_2 - a_2b_{12}$. Denote by $F_K^{-1}$ the inverse of $F_K$. Then we have

$$DF_K^{-1} \circ F_K(\xi,\eta) = \begin{pmatrix} \frac{\partial \xi}{\partial x} & \frac{\partial \xi}{\partial y} \\ \frac{\partial \eta}{\partial x} & \frac{\partial \eta}{\partial y} \end{pmatrix} = \frac{1}{J_K(\xi,\eta)} \begin{pmatrix} b_2 + b_{12}\xi & -a_2 - a_{12}\xi \\ -b_1 - b_{12}\eta & a_1 + a_{12}\eta \end{pmatrix}.$$

As pointed out in [54], we have the following elementary geometric properties.

**Lemma 2.2.** [54] *For any $K \in T_h$, under the shape regular hypothesis (5), we have*

$$\frac{\max\limits_{(\xi,\eta)\in\hat{K}} J_K(\xi,\eta)}{\min\limits_{(\xi,\eta)\in\hat{K}} J_K(\xi,\eta)} < \frac{h_K^2}{2\rho_K^2} \le \frac{\varrho^2}{2}, \tag{7}$$

$$a_{12}^2 + b_{12}^2 < \frac{1}{16}h_K^2, \tag{8}$$

$$\rho_K^2 < 4(a_1^2 + b_1^2) < h_K^2, \tag{9}$$

$$\rho_K^2 < 4(a_2^2 + b_2^2) < h_K^2. \tag{10}$$

**2.3. Hybrid FEM.** One can eliminate the stress $\boldsymbol{\sigma}$ in (2) to obtain a formulation involving only displacement $\boldsymbol{u}$ as the unknown. Then traditional Lagrange finite element spaces can be used to approximate the displacement. The stress approximation will be recovered by taking derivatives of the displacement approximation. There are two drawbacks along this direction. First, the recovered stress is less accurate. Second, for standard lower order elements, locking phenomenon could occur when $\lambda \to \infty$ as $\nu \to 0.5$, i.e., when the material is nearly incompressible. Mathematical understanding of locking effects can be found in [1, 5, 42].

Mixed methods based on Hellinger–Reissner variational principle approximating both stress and displacement can overcome these difficulties. The construction of a conforming or nonconforming and symmetric finite element spaces for the stress tensor, however, turns out to be highly non-trivial [2, 3, 4, 23, 49], since the weak solution, $(\boldsymbol{\sigma}, \boldsymbol{u})$, of the problem (2) is required to be in $H(\mathbf{div}, \Omega; \mathbb{R}^{d\times d}_{\text{sym}}) \times L^2(\Omega)^d$ for $d = 2$ or 3. The desirable stress

elements requires a large number of degrees of freedom, e.g. 24 for a low order conforming triangular element [3] and 162 for a conforming tetrahedral element [2]!

Another kind of mixed formulations widely used in engineering is the hybrid FEM based on the domain-decomposed Hellinger–Reissner principle [31, 32, 33, 34, 35, 36, 48, 50, 51, 53, 56], where the weak solution, $(\boldsymbol{\sigma}, \boldsymbol{u})$, of the problem (2) is required to be in $L^2(\Omega; \mathbb{R}^{d\times d}_{\text{sym}}) \times H^1(\Omega)^d$. In [32] Pian and Sumihara proposed a hybrid stress quadrilateral FEM (abbr. PS) which produces more accurate solutions than the traditional low order displacement finite elements and free from Poisson-locking. Xie and Zhou [50] presented a new hybrid stress finite element (called ECQ4) by using a different stress mode. This element was also shown by numerical benchmark tests to be locking-free and can produce even more accurate approximation solutions than PS element, especially when $\lambda$ is large.

We now give a brief introduction of the hybrid FEM. For simplicity we abbreviate the symmetric tensor $\boldsymbol{\tau} = \begin{pmatrix} \tau_{11} & \tau_{12} \\ \tau_{12} & \tau_{22} \end{pmatrix}$ to $\boldsymbol{\tau} = (\tau_{11}, \tau_{22}, \tau_{12})^t$. The 5-parameters stress mode on $\hat{K}$ for PS element [32] is

$$\hat{\boldsymbol{\tau}} = \begin{pmatrix} \hat{\boldsymbol{\tau}}_{11} \\ \hat{\boldsymbol{\tau}}_{22} \\ \hat{\boldsymbol{\tau}}_{12} \end{pmatrix} = \begin{pmatrix} 1 & 0 & 0 & \eta & \frac{a_2^2}{b_2^2}\xi \\ 0 & 1 & 0 & \frac{b_1^2}{a_1^2}\eta & \xi \\ 0 & 0 & 1 & \frac{b_1}{a_1}\eta & \frac{a_2}{b_2}\xi \end{pmatrix} \beta^{\boldsymbol{\tau}},\ \beta^{\boldsymbol{\tau}} \in \mathbb{R}^{\mathbf{5}}, \tag{11}$$

and the 5-parameters stress mode for ECQ4 element [50] is

$$\hat{\boldsymbol{\tau}} = \begin{pmatrix} \hat{\boldsymbol{\tau}}_{11} \\ \hat{\boldsymbol{\tau}}_{22} \\ \hat{\boldsymbol{\tau}}_{12} \end{pmatrix} = \begin{pmatrix} 1-\frac{b_{12}}{b_2}\xi & \frac{a_{12}a_2}{b_2^2}\xi & \frac{a_{12}b_2-a_2b_{12}}{b_2^2}\xi & \eta & \frac{a_2^2}{b_2^2}\xi \\ \frac{b_1b_{12}}{a_1^2}\eta & 1-\frac{a_{12}}{a_1}\eta & \frac{a_1b_{12}-a_{12}b_1}{a_1^2}\eta & \frac{b_1^2}{a_1^2}\eta & \xi \\ \frac{b_{12}}{a_1}\eta & \frac{a_{12}}{b_2}\xi & 1-\frac{b_{12}}{b_2}\xi-\frac{a_{12}}{a_1}\eta & \frac{b_1}{a_1}\eta & \frac{a_2}{b_2}\xi \end{pmatrix} \beta^{\boldsymbol{\tau}}. \tag{12}$$

Denote

$$\Sigma := \{\boldsymbol{\tau} \in L^2(\Omega; \mathbb{R}^{2\times 2}_{\text{sym}}) : \int_\Omega \text{tr}(\boldsymbol{\tau}) \text{d}x\text{d}y = 0\}.$$

Then the corresponding stress spaces for PS and ECQ4 elements are

$$\Sigma_h^{PS} = \{\boldsymbol{\tau} \in \Sigma :\ \hat{\boldsymbol{\tau}} = \boldsymbol{\tau}|_K \circ F_K \text{ is of the form of (11) for all } K \in \mathcal{T}_h\}, \tag{13}$$

$$\Sigma_h^{EC} = \{\boldsymbol{\tau} \in \Sigma :\ \hat{\boldsymbol{\tau}} = \boldsymbol{\tau}|_K \circ F_K \text{ is of the form of (12) for all } K \in \mathcal{T}_h\}. \tag{14}$$

In the following sections, we use one symbol $\Sigma_h$ for either $\Sigma_h^{PS}$ or $\Sigma_h^{EC}$. When all quadrilaterals are parallelograms, PS and ECQ4 elements are equivalent since $a_{12} = b_{12} = 0$.

For elements PS and ECQ4, the piecewise isoparametric bilinear interpolation is used for the displacement approximation, i.e. the displacement space $V_h$ is defined as

$$V_h = \{\boldsymbol{v} \in H_0^1(\Omega)^2 :\ \hat{\boldsymbol{v}} = \boldsymbol{v}|_K \circ F_K \in Q_1(\hat{K})^2 \text{ for all } K \in \mathcal{T}_h\}, \tag{15}$$

where $Q_1(\hat{K})$ denotes the set of bilinear polynomials on $\hat{K}$.

The hybrid stress FEM is formulated as: Find $(\boldsymbol{\sigma}_h, \boldsymbol{u}_h) \in \Sigma_h \times V_h$ such that

$$a(\boldsymbol{\sigma}_h, \boldsymbol{\tau}_h) + b(\boldsymbol{u}_h, \boldsymbol{\tau}_h) = 0 \qquad \text{for all } \boldsymbol{\tau}_h \in \Sigma_h, \tag{16}$$

$$b(\boldsymbol{v}_h, \boldsymbol{\sigma}_h) = -f(\boldsymbol{v}_h) \qquad \text{for all } \boldsymbol{v}_h \in V_h, \tag{17}$$

where

$$a(\boldsymbol{\sigma}, \boldsymbol{\tau}) = \int_\Omega \boldsymbol{\tau} : (\mathbb{C}^{-1}\boldsymbol{\sigma}) \mathrm{d}x\mathrm{d}y = \frac{1}{2\mu}\int_\Omega \left( \boldsymbol{\sigma} : \boldsymbol{\tau} - \frac{\lambda}{2(\mu+\lambda)} \mathrm{tr}(\boldsymbol{\sigma})\mathrm{tr}(\boldsymbol{\tau}) \right) \mathrm{d}x\mathrm{d}y, \tag{18}$$

$$b(\boldsymbol{v}, \boldsymbol{\tau}) = -\int_\Omega \epsilon(\boldsymbol{v}) : \boldsymbol{\tau} \mathrm{d}x\mathrm{d}y, \tag{19}$$

$$f(\boldsymbol{v}) = \int_\Omega \boldsymbol{f} \cdot \boldsymbol{v} \mathrm{d}x\mathrm{d}y. \tag{20}$$

The classical analysis of hybrid FEM can be found in Zhou and Xie [56]. Recently Yu, Xie and Carstensen [52] gave a rigorous uniform convergence analysis for PS and ECQ4 elements. We shall mainly follow their approach to prove the inf-sup conditions.

## 3. Hybrid FVM

This section is devoted to the construction of a hybrid stress FVM which is a coupling version of FVM and hybrid stress FEM based on PS or ECQ4 stress mode. We will use FVM for the equilibrium equation (the first equation in (2)) and use FEM for the constitutive equation (the second equation in (2)).

Let $\{X_i = (x_i, y_i),\ 1 \le i \le N\}$ be the interior nodes set of $\mathcal{T}_h$, where $N$ denotes the number of interior nodes. We construct a dual partition $\mathcal{T}_h^* = \{K_i^*,\ 1 \le i \le N\}$, where $K_i^*$ is the dual element (control volume) of the node $X_i$ shown in Figure 2(a). In this figure, $O_{il},\ 1 \le l \le 4$ are the centers of the $l-$th quadrilateral element neighboring to $X_i$, which are mapping from the center of the reference element $\hat{K}$ by bilinear transformations, and $M_{il},\ 1 \le l \le 4$ are midpoints of all edges connected with $X_i$. In addition, for all quadrilateral elements $K \in \mathcal{T}_h$, we call the restriction region $D_l^K$ of the dual element $K_{il}^*,\ 1 \le l \le 4$ in $K$ as the $l-$th control sub-volume of $K$; see Figure 2(b).

Define a piecewise constant vector space $V_h^*$ on $\mathcal{T}_h^*$ as

$$V_h^* := \{\boldsymbol{v} \in (L^2(\Omega))^2 :\ \boldsymbol{v}|_{K_i^*} \text{ is a constant vector, for all } 1 \le i \le N\}. \tag{21}$$

By the definition, we can easily check that $\dim V_h^* = \dim V_h$.

We first present a weak form coupling FEM and FVM: Find $(\boldsymbol{\sigma}_h, \boldsymbol{u}_h) \in \Sigma_h \times V_h$, such that

$$a(\boldsymbol{\sigma}_h, \boldsymbol{\tau}) + b(\boldsymbol{u}_h, \boldsymbol{\tau}) = 0 \qquad \text{for all } \boldsymbol{\tau} \in \Sigma_h, \tag{22}$$

$$c(\boldsymbol{v}_*, \boldsymbol{\sigma}_h) = f(\boldsymbol{v}_*) \qquad \text{for all } \boldsymbol{v}_* \in V_h^*, \tag{23}$$

where $a(\cdot,\cdot)$, $b(\cdot,\cdot)$ and $f(\cdot)$ are defined in (18)-(20), respectively, and

$$c(\boldsymbol{v}_*, \boldsymbol{\sigma}_h) = -\sum_{K \in \mathcal{T}_h} \sum_{i=1}^{N} \int_{\partial K_i^* \cap K} \boldsymbol{\sigma}_h \boldsymbol{n} \cdot \boldsymbol{v}_* \mathrm{d}s.$$

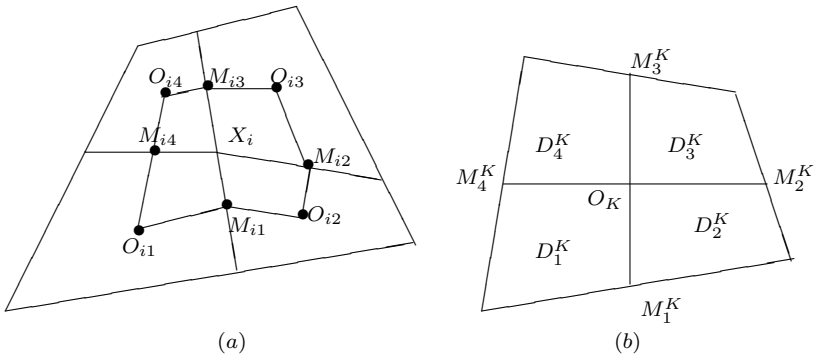


FIGURE 2. (a) Dual element $K_i^*$ $(O_{i1}M_{i1}O_{i2}M_{i2}O_{i3}M_{i3}O_{i4}M_{i4})$ of the node $X_i$. (b) Quadrilateral element $K \in \mathcal{T}_h$ and its four sub-volumes, where $M_i^K$ $(i = 1, \cdots, 4)$ are the mid-points of the four edges of $K$ and $O_K$ is the center of $K$.

We introduce a minor modification of the bilinear form $b(\cdot, \cdot)$, i.e.

$$\tilde{b}(\boldsymbol{u}_h, \boldsymbol{\tau}) = -\int_\Omega \tilde{\epsilon}(\boldsymbol{u}_h) : \boldsymbol{\tau} \mathrm{d}x\mathrm{d}y.$$

Here, by following [54], the modified strain tensor $\tilde{\epsilon}(\boldsymbol{v})$ is defined as

$$\tilde{\epsilon}(\boldsymbol{v}) = \begin{pmatrix} \frac{\tilde{\partial} u}{\partial x} & \frac{1}{2}(\frac{\tilde{\partial} u}{\partial y} + \frac{\tilde{\partial} v}{\partial x}) \\ \frac{1}{2}(\frac{\tilde{\partial} u}{\partial y} + \frac{\tilde{\partial} v}{\partial x}) & \frac{\tilde{\partial} v}{\partial y} \end{pmatrix},$$

with the modified partial derivatives $\frac{\tilde{\partial} v}{\partial x}$, $\frac{\tilde{\partial} v}{\partial y}$ on $K \in \mathcal{T}_h$ given by

$$(J_K \frac{\tilde{\partial} v}{\partial x}|_K \circ F_K)(\xi, \eta) = \frac{\partial y}{\partial \eta}(0,0)\frac{\partial \hat{v}}{\partial \xi} - \frac{\partial y}{\partial \xi}(0,0)\frac{\partial \hat{v}}{\partial \eta} = b_2 \frac{\partial \hat{v}}{\partial \xi} - b_1 \frac{\partial \hat{v}}{\partial \eta},$$

$$(J_K \frac{\tilde{\partial} v}{\partial y}|_K \circ F_K)(\xi, \eta) = -\frac{\partial x}{\partial \eta}(0,0)\frac{\partial \hat{v}}{\partial \xi} + \frac{\partial x}{\partial \xi}(0,0)\frac{\partial \hat{v}}{\partial \eta} = -a_2 \frac{\partial \hat{v}}{\partial \xi} + a_1 \frac{\partial \hat{v}}{\partial \eta}.$$

Let $\chi_i$ $(1 \le i \le N)$ be the characteristic function on $K_i^*$, and $\varphi_i$ $(1 \le i \le N)$ the nodal base of the interior node $X_i$. We define a mapping $r_h : V_h \to V_h^*$ by

$$r_h \boldsymbol{v} = \sum_{i=1}^N \alpha_i \chi_i, \qquad \text{for all } \boldsymbol{v} = \sum_{i=1}^N \alpha_i \varphi_i \in V_h. \tag{24}$$

It is easy to see that $r_h$ is a one to one and onto operator from $V_h$ to $V_h^*$. We can then pull back the bilinear form $c(\cdot, \cdot)$ defined on $V_h^* \times \Sigma_h$ to $V_h \times \Sigma_h$ by the mapping $r_h$, i.e.

$$c(\boldsymbol{v}, \boldsymbol{\sigma}_h) := c(r_h \boldsymbol{v}, \boldsymbol{\sigma}_h) \qquad \text{for all } \boldsymbol{v} \in V_h,\ \boldsymbol{\sigma}_h \in \Sigma_h. \tag{25}$$

Our hybrid stress FVM is based on the following modified weak form: Find $(\boldsymbol{\sigma}_h, \boldsymbol{u}_h) \in \Sigma_h \times V_h$, such that

$$a(\boldsymbol{\sigma}_h, \boldsymbol{\tau}) + \tilde{b}(\boldsymbol{u}_h, \boldsymbol{\tau}) = 0 \qquad \text{for all } \boldsymbol{\tau} \in \Sigma_h, \tag{26}$$

$$c(\boldsymbol{v}, \boldsymbol{\sigma}_h) = f(r_h \boldsymbol{v}) \qquad \text{for all } \boldsymbol{v} \in V_h. \tag{27}$$

Note that (26) is still in the FEM form while in (27), by choosing $\boldsymbol{v}_* = \chi_{K_i}$, the equilibrium equation

$$-\int_{\partial K_i^*} \boldsymbol{\sigma}_h n \, \mathrm{d}s = \int_{K_i^*} f \, \mathrm{d}x$$

holds in each control volume $K_i^*$, i.e., it is in the FVM form.

Define $\mathcal{A} : \Sigma_h \to \Sigma_h$ as

$$a(\boldsymbol{\sigma}, \boldsymbol{\tau}) = (\mathcal{A}\boldsymbol{\sigma},\ \boldsymbol{\tau}) \quad \text{for all } \boldsymbol{\sigma} \in \Sigma_h,\ \boldsymbol{\tau} \in \Sigma_h,$$

$\tilde{\mathcal{B}}^t : V_h \to \Sigma_h$ and $\tilde{\mathcal{B}} : \Sigma_h \to V_h$ as

$$\tilde{b}(\boldsymbol{v}, \boldsymbol{\tau}) = (\tilde{\mathcal{B}}^t \boldsymbol{v},\ \boldsymbol{\tau}) = (\boldsymbol{v},\ \tilde{\mathcal{B}}\boldsymbol{\tau}) \quad \text{for all } \boldsymbol{v} \in V_h,\ \boldsymbol{\tau} \in \Sigma_h,$$

$\mathcal{C}^t : V_h \to \Sigma_h$ and $\mathcal{C} : \Sigma_h \to V_h$ as

$$c(\boldsymbol{v}, \boldsymbol{\tau}) = (\mathcal{C}^t \boldsymbol{v},\ \boldsymbol{\tau}) = (\boldsymbol{v},\ \mathcal{C}\boldsymbol{\tau}) \quad \text{for all } \boldsymbol{v} \in V_h,\ \boldsymbol{\tau} \in \Sigma_h,$$

and $\tilde{\boldsymbol{f}} : V_h \to \mathbb{R}$ as $(\tilde{\boldsymbol{f}}, \boldsymbol{v}) = f(r_h \boldsymbol{v})$.

We can write (26)-(27) in the form of

$$\begin{pmatrix} \mathcal{A} & \tilde{\mathcal{B}}^t \\ \mathcal{C} & 0 \end{pmatrix} \begin{pmatrix} \boldsymbol{\sigma} \\ \boldsymbol{u} \end{pmatrix} = \begin{pmatrix} 0 \\ \tilde{\boldsymbol{f}} \end{pmatrix} \tag{28}$$

In the following sections, we will focus on our new FVM method based on the modified weak forms (26)-(27) or equivalently the saddle point system (28).

## 4. Stability analysis

This section is to establish some stability results which are uniform with respect to the Lamé constant $\lambda$ and get the well-posedness of (26)-(27). We shall focus on PS stress mode first and then use a perturbation argument to prove similar results for ECQ4 stress mode.

According to the mixed FEM theory [8, 10], we need to establish several inf-sup conditions and continuity conditions.

- Kernel inf-sup conditions: There exists a constant $\alpha_1 > 0$ independent of $h$, $\lambda$ such that

$$\sup_{\boldsymbol{\tau} \in \ker(\tilde{\mathcal{B}})} \frac{a(\boldsymbol{\sigma}, \boldsymbol{\tau})}{\|\boldsymbol{\tau}\|} \geq \alpha_1 \|\boldsymbol{\sigma}\| \qquad \text{for all } \boldsymbol{\sigma} \in \ker(\mathcal{C}), \tag{29}$$

$$\sup_{\boldsymbol{\sigma} \in \ker(\mathcal{C})} a(\boldsymbol{\sigma}, \boldsymbol{\tau}) > 0 \qquad \text{for all } \boldsymbol{\tau} \in \ker(\tilde{\mathcal{B}}) \setminus \{0\}. \tag{30}$$

  As pointed out in [8], by Open Mapping Theorem the above statement is also equivalent to the existence of a constant $\alpha_2 > 0$ independent of $h$, $\lambda$ such that

$$\sup_{\boldsymbol{\sigma} \in \ker(\mathcal{C})} \frac{a(\boldsymbol{\sigma}, \boldsymbol{\tau})}{\|\boldsymbol{\sigma}\|} \geq \alpha_2 \|\boldsymbol{\tau}\| \qquad \text{for all } \boldsymbol{\tau} \in \ker(\tilde{\mathcal{B}}), \tag{31}$$

$$\sup_{\boldsymbol{\tau} \in \ker(\tilde{\mathcal{B}})} a(\boldsymbol{\sigma}, \boldsymbol{\tau}) > 0 \qquad \text{for all } \boldsymbol{\sigma} \in \ker(\mathcal{C}) \setminus \{0\}. \tag{32}$$

In a finite dimensional case (30) and (32) can be replaced by

$$\dim(\ker(\tilde{\mathcal{B}})) = \dim(\ker(\mathcal{C})). \tag{33}$$

- Discrete inf-sup conditions for $\tilde{b}$ and $c$: For any $\boldsymbol{v} \in V_h$, it holds

$$|\boldsymbol{v}|_1 \lesssim \sup_{0\neq\boldsymbol{\tau}\in\Sigma_h} \frac{\tilde{b}(\boldsymbol{v},\boldsymbol{\tau})}{\|\boldsymbol{\tau}\|}, \tag{34}$$

$$|\boldsymbol{v}|_1 \lesssim \sup_{0\neq\boldsymbol{\tau}\in\Sigma_h} \frac{c(\boldsymbol{v},\boldsymbol{\tau})}{\|\boldsymbol{\tau}\|}. \tag{35}$$

- Continuity conditions: For any $\boldsymbol{v} \in V_h$, $\boldsymbol{\sigma},\ \boldsymbol{\tau} \in \Sigma_h$, it holds

$$a(\boldsymbol{\sigma},\boldsymbol{\tau}) \lesssim \|\boldsymbol{\sigma}\|\|\boldsymbol{\tau}\|, \tag{36}$$

$$\tilde{b}(\boldsymbol{v},\boldsymbol{\tau}) \lesssim |\boldsymbol{v}|_1\|\boldsymbol{\tau}\|, \tag{37}$$

$$c(\boldsymbol{v},\boldsymbol{\tau}) \lesssim |\boldsymbol{v}|_1\|\boldsymbol{\tau}\|. \tag{38}$$

**4.1. Continuity conditions.** The continuity conditions (36) and (37) are easy to prove; see, for example, [52]. We only give a proof of (38).

**Theorem 4.1.** *For any $\boldsymbol{v} \in V_h$ and $\boldsymbol{\tau} \in \Sigma_h$, the uniform continuity condition (38) holds.*

*Proof.* For any $\boldsymbol{v} \in V_h$ and $\boldsymbol{\tau} \in \Sigma_h$, we have

$$\begin{aligned}
c(\boldsymbol{v},\boldsymbol{\tau}) &= -\sum_{K\in\mathcal{T}_h}\sum_{i=1}^{N}\int_{\partial K_i^*\cap K} \boldsymbol{\tau}\boldsymbol{n}\cdot r_h\boldsymbol{v}\mathrm{d}s = \sum_{K\in\mathcal{T}_h}\sum_{i=1}^{N}\int_{\partial K_i^*\cap K} \boldsymbol{\tau}\boldsymbol{n}\cdot(\boldsymbol{v}-r_h\boldsymbol{v})\mathrm{d}s\\
&\lesssim \sum_{K\in\mathcal{T}_h}\sum_{i=1}^{N}\left(\int_{\partial K_i^*\cap K}|\boldsymbol{v}-r_h\boldsymbol{v}|^2\mathrm{d}s\right)^{1/2}\left(\int_{\partial K_i^*\cap K}|\boldsymbol{\tau}|^2\mathrm{d}s\right)^{1/2}\\
&\lesssim \sum_{K\in\mathcal{T}_h}(h_K^{-1}\|\boldsymbol{v}-r_h\boldsymbol{v}\|_{0,K}^2 + h_K\sum_{j=1}^{4}|\boldsymbol{v}-r_h\boldsymbol{v}|_{1,D_j^K}^2)^{1/2}(h_K^{-1}\|\boldsymbol{\tau}\|_{0,K}^2+h_K|\boldsymbol{\tau}|_{1,K}^2)^{1/2}\\
&\lesssim \sum_{K\in\mathcal{T}_h}|\boldsymbol{v}|_{1,K}\|\boldsymbol{\tau}\|_{0,K} \lesssim |\boldsymbol{v}|_1\|\boldsymbol{\tau}\|,
\end{aligned}$$

where in the second identity we have used the fact that $\sum_{K\in\mathcal{T}_h}\sum_{i=1}^{N}\int_{\partial K_i^*\cap K}\boldsymbol{\tau}\boldsymbol{n}\cdot\boldsymbol{v} = 0$ since $\boldsymbol{v} \in V_h \subset H^1(\Omega)^2$ and $\boldsymbol{\tau}$ is a polynomial tensor inside an element $K \in \mathcal{T}_h$, and in the last inequality we have used the estimate ( [13], Lemma 2.4)

$$\|\boldsymbol{v}-r_h\boldsymbol{v}\|_{0,K} \lesssim h_K|\boldsymbol{v}|_{1,K} \qquad \text{for all } \boldsymbol{v}\in V_h.$$

□

**4.2. Kernel inf-sup conditions.** We will first verify the dimension of the null space of $\tilde{\mathcal{B}}$ and $\mathcal{C}$ equals. Then we prove the inf-sup conditions (29) and (31) by choosing $\tau = \sigma$. We will make use of the following special relation of the matrix $\tilde{\mathcal{B}}$ and $\mathcal{C}$.

**Theorem 4.2.** *For PS stress mode, there exists a symmetric and positive definite matrix $\mathcal{D}$ such that $\tilde{\mathcal{B}} = \mathcal{D}\mathcal{C}$. Therefore ker$(\tilde{\mathcal{B}})$ = ker$(\mathcal{C})$.*

As a consequence of Theorem 4.2, we can rewrite our discretization based on PS stress mode as

$$\begin{pmatrix} \mathcal{A} & \tilde{\mathcal{B}}^t \\ \tilde{\mathcal{B}} & 0 \end{pmatrix} \begin{pmatrix} \boldsymbol{\sigma} \\ \boldsymbol{u} \end{pmatrix} = \begin{pmatrix} 0 \\ \mathcal{D}\tilde{\boldsymbol{f}} \end{pmatrix}. \tag{39}$$

Namely we obtain the same matrix as the (modified) hybrid FEM but a different way to assemble the load. An analog result of the linear finite volume method for the Poisson equation was established in [7, 21, 39].

Since $\Sigma_h$ is piecewise independent, we can easily eliminate $\boldsymbol{\sigma}$ and obtain a symmetric and positive definite system for which we can use multigrid methods to compute the solution in a fast way. The size of the SPD problem is the same as that from the displacement method using the isoparametric bilinear element.

The proof of Theorem 4.2 is technical. The idea is to calculate the element-wise matrix. We first follow [52] to introduce some notation. Denote

$$\Phi = \begin{pmatrix} 1 & \xi & \eta & 0 & 0 & 0 & 0 & 0 & 0 \\ 0 & 0 & 0 & 1 & \xi & \eta & 0 & 0 & 0 \\ 0 & 0 & 0 & 0 & 0 & 0 & 1 & \xi & \eta \end{pmatrix}.$$

On an element $K \in \mathcal{T}_h$, we can rewrite (11) and (12) as $\begin{pmatrix} \hat{\boldsymbol{\tau}}_{11} \\ \hat{\boldsymbol{\tau}}_{22} \\ \hat{\boldsymbol{\tau}}_{12} \end{pmatrix} = \Phi A \beta^{\boldsymbol{\tau}}$, where for PS stress form,

$$A = A_{PS} = \begin{pmatrix} 1 & 0 & 0 & 0 & 0 \\ 0 & 0 & 0 & 0 & \frac{a_2^2}{b_2^2} \\ 0 & 0 & 0 & 1 & 0 \\ 0 & 1 & 0 & 0 & 0 \\ 0 & 0 & 0 & 0 & 1 \\ 0 & 0 & 0 & \frac{b_1^2}{a_1^2} & 0 \\ 0 & 0 & 1 & 0 & 0 \\ 0 & 0 & 0 & 0 & \frac{a_2}{b_2} \\ 0 & 0 & 0 & \frac{b_1}{a_1} & 0 \end{pmatrix},$$

and for ECQ4 stress form,

$$A = A_{EC} = A_{PS} + \begin{pmatrix} 0 & 0 & 0 & 0 & 0 \\ -\frac{b_{12}}{b_2} & \frac{a_{12}a_2}{b_2^2} & \frac{a_{12}b_2 - a_2 b_{12}}{b_2^2} & 0 & 0 \\ 0 & 0 & 0 & 0 & 0 \\ 0 & 0 & 0 & 0 & 0 \\ 0 & 0 & 0 & 0 & 0 \\ \frac{b_1 b_{12}}{a_1^2} & -\frac{a_{12}}{a_1} & \frac{a_1 b_{12} - a_{12} b_1}{a_1^2} & 0 & 0 \\ 0 & 0 & 0 & 0 & 0 \\ 0 & \frac{a_{12}}{b_2} & -\frac{b_{12}}{b_2} & 0 & 0 \\ \frac{b_{12}}{a_1} & 0 & -\frac{a_{12}}{a_1} & 0 & 0 \end{pmatrix} =: A_{PS} + \delta_A^K. \tag{40}$$

When the quadrilateral is a parallelogram, $\delta_A^K = 0$ since $a_{12} = b_{12} = 0$. In general, the non-zero element of $A_{PS}$ is $O(1)$, and the non-zero elements of $\delta_A^K$ is $o(1)$ when condition (A) is satisfied. Therefore $\delta_A^K$ is considered as a high order perturbation.

For any $\boldsymbol{v} = (u, v)^t \in V_h$ with nodal values $\boldsymbol{v}(Z_i) = (u_i, v_i)^t$ on $K \in \mathcal{T}_h$, let

$$\hat{\boldsymbol{v}} = \sum_{i=1}^{4} \begin{pmatrix} u_i \\ v_i \end{pmatrix} N_i(\xi, \eta) = \begin{pmatrix} U_0 + U_1\xi + U_2\eta + U_{12}\xi\eta \\ V_0 + V_1\xi + V_2\eta + V_{12}\xi\eta \end{pmatrix}, \tag{41}$$

where $N_i, 1 \le i \le 4$, are bases of bilinear function on $\hat{K}$

$$N_1(\xi,\eta) = \frac{1}{4}(1-\xi)(1-\eta),\ N_2(\xi,\eta) = \frac{1}{4}(1+\xi)(1-\eta),$$
$$N_3(\xi,\eta) = \frac{1}{4}(1+\xi)(1+\eta),\ N_4(\xi,\eta) = \frac{1}{4}(1-\xi)(1+\eta),$$

and

$$\begin{pmatrix} U_0 & V_0 \\ U_1 & V_1 \\ U_2 & V_2 \\ U_{12} & V_{12} \end{pmatrix} = \frac{1}{4} \begin{pmatrix} 1 & 1 & 1 & 1 \\ -1 & 1 & 1 & -1 \\ -1 & -1 & 1 & 1 \\ 1 & -1 & 1 & -1 \end{pmatrix} \begin{pmatrix} u_1 & v_1 \\ u_2 & v_2 \\ u_3 & v_3 \\ u_4 & v_4 \end{pmatrix}.$$

Then, we can write

$$\begin{aligned} & J_K \begin{pmatrix} \frac{\tilde{\partial} u}{\partial x} \\ \frac{\partial v}{\partial y} \\ \frac{\tilde{\partial} u}{\partial y} + \frac{\tilde{\partial} v}{\partial x} \end{pmatrix} \circ F_K \\ & = \Phi \begin{pmatrix} b_2 & -b_1 & 0 & 0 & 0 \\ 0 & 0 & -b_1 & 0 & 0 \\ 0 & 0 & b_2 & 0 & 0 \\ 0 & 0 & 0 & a_1 & 0 \\ 0 & 0 & 0 & 0 & a_1 \\ 0 & 0 & 0 & 0 & -a_2 \\ -a_2 & a_1 & 0 & -b_1 & 0 \\ 0 & 0 & a_1 & 0 & -b_1 \\ 0 & 0 & -a_2 & 0 & b_2 \end{pmatrix} \begin{pmatrix} U_1 + \frac{b_1}{a_1} V_1 \\ U_2 + \frac{b_2}{a_1} V_1 \\ U_{12} \\ V_2 - \frac{a_2}{a_1} V_1 \\ V_{12} \end{pmatrix} =: \Phi B v^5, \end{aligned}$$

with $v^5 = (U_1 + \frac{b_1}{a_1}V_1,\ U_2 + \frac{b_2}{a_1}V_1,\ U_{12},\ V_2 - \frac{a_2}{a_1}V_1,\ V_{12})^t$.

Using above notation, for any $\boldsymbol{\tau} \in \Sigma_h$, $\boldsymbol{v} \in V_h$ and $K \in \mathcal{T}_h$, it can be verified by direct calculation that

$$(\mathcal{C}_K \boldsymbol{\tau}, \boldsymbol{v})_K = -\sum_{i=1}^{N} \int_{\partial K_i^* \cap K} \boldsymbol{\tau}\boldsymbol{n} \cdot r_h \boldsymbol{v} \mathrm{d}s = (\beta^{\boldsymbol{\tau}})^t A^t H B v^5, \tag{42}$$

$$(\boldsymbol{\tau}, \tilde{\mathcal{B}}_K^t \boldsymbol{v})_K = \int_K \boldsymbol{\tau} : \tilde{\epsilon}(\boldsymbol{v}) \mathrm{d}x\mathrm{d}y = (\beta^{\boldsymbol{\tau}})^t A^t \tilde{H} B v^5, \tag{43}$$

where

$$H = \mathrm{diag}(4,2,2,4,2,2,4,2,2),$$
$$\tilde{H} = \frac{4}{3}\mathrm{diag}(3,1,1,3,1,1,3,1,1) = \int_{\hat{K}} \Phi^t \Phi \mathrm{d}\xi\mathrm{d}\eta.$$

For PS stress form,

(44)
$$A_{PS}^t HB = \begin{pmatrix} 4 & 0 & 0 & 0 & 0 \\ 0 & 4 & 0 & 0 & 0 \\ 0 & 0 & 4 & 0 & 0 \\ 0 & 0 & 0 & 2 & 0 \\ 0 & 0 & 0 & 0 & 2 \end{pmatrix} \begin{pmatrix} b_2 & -b_1 & 0 & 0 & 0 \\ 0 & 0 & 0 & a_1 & 0 \\ -a_2 & a_1 & 0 & -b_1 & 0 \\ 0 & 0 & \frac{J_0}{a_1} & 0 & \frac{b_1 J_0}{a_1^2} \\ 0 & 0 & \frac{a_2 J_0}{b_2^2} & 0 & \frac{J_0}{b_2} \end{pmatrix} =: DA_B,$$

(45)
$$A_{PS}^t \tilde{H}B = \begin{pmatrix} 4 & 0 & 0 & 0 & 0 \\ 0 & 4 & 0 & 0 & 0 \\ 0 & 0 & 4 & 0 & 0 \\ 0 & 0 & 0 & \frac{4}{3} & 0 \\ 0 & 0 & 0 & 0 & \frac{4}{3} \end{pmatrix} \begin{pmatrix} b_2 & -b_1 & 0 & 0 & 0 \\ 0 & 0 & 0 & a_1 & 0 \\ -a_2 & a_1 & 0 & -b_1 & 0 \\ 0 & 0 & \frac{J_0}{a_1} & 0 & \frac{b_1 J_0}{a_1^2} \\ 0 & 0 & \frac{a_2 J_0}{b_2^2} & 0 & \frac{J_0}{b_2} \end{pmatrix} =: \tilde{D}A_B.$$

For ECQ4 stress form,

(46)
$$A_{EC}^t HB = A_{PS}^t HB + 2\boldsymbol{\delta}_{EC}, \quad A_{EC}^t \tilde{H}B = A_{PS}^t \tilde{H}B + \frac{4}{3}\boldsymbol{\delta}_{EC},$$

where

(47)
$$\boldsymbol{\delta}_{EC} = \begin{pmatrix} 0 & 0 & -b_{12}\frac{a_1 b_1 - a_2 b_2}{a_1 b_2} & 0 & \frac{b_{12}}{a_1^2} J_0 \\ 0 & 0 & \frac{a_{12}}{b_2^2} J_0 & 0 & \frac{a_{12}}{a_1 b_2}(a_2 b_2 - a_1 b_1) \\ 0 & 0 & \frac{a_2 a_{12}}{a_1} - \frac{b_1}{b_2^2} J_2 - \frac{a_1 b_{12}}{b_2} & 0 & \frac{b_1 b_{12}}{b_2} - \frac{a_2 J_1}{a_1^2} - \frac{a_{12} b_2}{a_1} \\ 0 & 0 & 0 & 0 & 0 \\ 0 & 0 & 0 & 0 & 0 \end{pmatrix}.$$

Now we are in the position to prove Theorem 4.2.

*Proof.* Define $\mathscr{V} = (u_1, u_2, u_3, u_4, v_1, v_2, v_3, v_4)^t$, $\mathscr{U} = (U_0,\, U_1,\, U_2,\, U_{12},\, V_0,\, V_1,\, V_2,\, V_{12})^t$,

$$G = \begin{pmatrix} 0 & 1 & 0 & 0 & 0 & \frac{b_1}{a_1} & 0 & 0 \\ 0 & 0 & 1 & 0 & 0 & \frac{b_2}{a_1} & 0 & 0 \\ 0 & 0 & 0 & 1 & 0 & 0 & 0 & 0 \\ 0 & 0 & 0 & 0 & 0 & -\frac{a_2}{a_1} & 1 & 0 \\ 0 & 0 & 0 & 0 & 0 & 0 & 0 & 1 \end{pmatrix}, T = \begin{pmatrix} 1 & 1 & 1 & 1 & 0 & 0 & 0 & 0 \\ -1 & 1 & 1 & -1 & 0 & 0 & 0 & 0 \\ -1 & -1 & 1 & 1 & 0 & 0 & 0 & 0 \\ 1 & -1 & 1 & -1 & 0 & 0 & 0 & 0 \\ 0 & 0 & 0 & 0 & 1 & 1 & 1 & 1 \\ 0 & 0 & 0 & 0 & -1 & 1 & 1 & -1 \\ 0 & 0 & 0 & 0 & -1 & -1 & 1 & 1 \\ 0 & 0 & 0 & 0 & 1 & -1 & 1 & -1 \end{pmatrix}.$$

Some simple calculations show

$$v^5 = (U_1 + \frac{b_1}{a_1}V_1,\, U_2 + \frac{b_2}{a_1}V_1,\, U_{12},\, V_2 - \frac{a_2}{a_1}V_1,\, V_{12})^t = G\mathscr{U} = \frac{1}{4}GT\mathscr{V}.$$

Using (44) and (45), we see that, for PS stress mode, the matrices $\tilde{\mathcal{B}}$ and $\mathcal{C}$ restricted on $K \in \mathcal{T}_h$ are of the forms

$$\tilde{\mathcal{B}}_K = \frac{1}{4}T^t G^t A_B^t \tilde{D} = \frac{1}{4}T^t \mathrm{diag}(4,4,4,\frac{4}{3},4,4,4,\frac{4}{3})G^t A_B^t,$$
$$\mathcal{C}_K = \frac{1}{4}T^t G^t A_B^t D = \frac{1}{4}T^t \mathrm{diag}(4,4,4,2,4,4,4,2)G^t A_B^t.$$

Let $\mathcal{D}_K := \frac{1}{4}T^t\text{diag}(1,1,1,\frac{2}{3},1,1,1,\frac{2}{3})T$. Since $TT^t = 4I_{8\times 8}$, where $I_{8\times 8}$ is an identity matrix, it holds

$$\tilde{\mathcal{B}}_K = \mathcal{D}_K\mathcal{C}_K.$$

Thus, we obtain $\tilde{\mathcal{B}} = \mathcal{D}\mathcal{C}$. The matrix $\mathcal{D}$ is symmetric and positive definite from the fact that $\mathcal{D}_K$ is symmetric and positive defined. □

**Condition (C).** The $Q_1 - P_0$ inf-sup condition for Stokes equations holds, i.e., for all $q \in \bar{W}_h := \{q \in L^2(\Omega) : \ q|_K \in P_0 \ \text{ for all } K \in \mathcal{T}_h\}$

$$\|q\| \lesssim \sup_{\boldsymbol{v}\in V_h} \frac{\int_\Omega \text{div}\boldsymbol{v}\, q\, \mathrm{d}x\mathrm{d}y}{|\boldsymbol{v}|_1}. \tag{48}$$

It is well known that the only unstable case for $Q_1 - P_0$ for Stokes equations is the checkerboard mode. So any quadrilateral mesh which breaks the checkerboard mode is sufficient for the uniform coercivity condition (49).

The proof of the following lemma can be found in [52].

**Lemma 4.3.** *([52]) Let the partition $\mathcal{T}_h$ satisfy the shape regular condition (5) and the condition (C). Then for PS stress mode, it holds the uniform coercivity condition*

$$a(\boldsymbol{\tau},\boldsymbol{\tau}) \gtrsim \|\boldsymbol{\tau}\|^2 \qquad \textit{for all } \boldsymbol{\tau} \in \textit{ker}(\tilde{\mathcal{B}}). \tag{49}$$

By Theorem 4.2 and Lemma 4.3, we can take $\sigma = \tau$ in (29) to get the following theorem.

**Theorem 4.4.** *Let the partition $\mathcal{T}_h$ satisfy the shape regular condition (5) and the condition (C). Then the uniform discrete kernel inf-sup conditions (29) and (31) hold.*

**4.3. Discrete inf-sup conditions.** We show the following results for $\tilde{b}(\cdot,\cdot)$and $c(\cdot,\cdot)$.

**Theorem 4.5.** *Let the partition $\{\mathcal{T}_h\}_{h>0}$ satisfy the shape regularity condition (5). Then for PS stress mode the uniform discrete inf-sup conditions (34) and (35) hold.*

*Proof.* It suffices to prove that for any $\boldsymbol{v} \in V_h$, there exists $\boldsymbol{\tau}_{\boldsymbol{v}} \in \Sigma_h$ such that

$$\|\tilde{\epsilon}(\boldsymbol{v})\|_{0,K}^2 \lesssim \|\boldsymbol{\tau}_{\boldsymbol{v}}\|_{0,K}^2 \lesssim \min\left\{\int_K \tilde{\epsilon}(\boldsymbol{v}) : \boldsymbol{\tau}_{\boldsymbol{v}}\mathrm{d}x\mathrm{d}y, -\sum_{i=1}^N \int_{\partial K_i^*\cap K} \boldsymbol{\tau}_{\boldsymbol{v}}\boldsymbol{n}\cdot r_h\boldsymbol{v}\mathrm{d}s\right\}. \tag{50}$$

In fact, if (50) holds, by the Korn inequality, we have

$$\begin{aligned}\|\boldsymbol{\tau}_{\boldsymbol{v}}\||\boldsymbol{v}|_1 &\lesssim \left(\sum_{K\in\mathcal{T}_h}\|\boldsymbol{\tau}_{\boldsymbol{v}}\|_{0,K}^2\right)^{1/2}\left(\sum_{K\in\mathcal{T}_h}\|\tilde{\epsilon}(\boldsymbol{v})\|_{0,K}^2\right)^{1/2}\\ &\lesssim \sum_{K\in\mathcal{T}_h}\|\boldsymbol{\tau}_{\boldsymbol{v}}\|_{0,K}^2 \lesssim \int_K \tilde{\epsilon}(\boldsymbol{v}) : \boldsymbol{\tau}_{\boldsymbol{v}}\mathrm{d}x\mathrm{d}y,\end{aligned}$$

and similarly

$$\|\boldsymbol{\tau}_{\boldsymbol{v}}\||\boldsymbol{v}|_1 \lesssim \sum_{K\in\mathcal{T}_h}\|\boldsymbol{\tau}_{\boldsymbol{v}}\|_{0,K}^2 \lesssim -\sum_{K\in\mathcal{T}_h}\sum_{i=1}^N\int_{\partial K_i^*\cap K}\boldsymbol{\tau}_{\boldsymbol{v}}\boldsymbol{n}\cdot r_h\boldsymbol{v}\mathrm{d}s.$$

Then the inf-sup conditions (34) and (35) follow.

Now we turn to prove (50). For any $\boldsymbol{v} \in V_h$, $K \in \mathcal{T}_h$, taking $\boldsymbol{\tau_v} \in \Sigma_h$ as

$$[\hat{\boldsymbol{\tau}}_{\boldsymbol{v}11}, \hat{\boldsymbol{\tau}}_{\boldsymbol{v}22}, \hat{\boldsymbol{\tau}}_{\boldsymbol{v}12}]^t = \Phi A_{PS} \beta_{\boldsymbol{v}}$$

with $\beta_{\boldsymbol{v}} = \frac{1}{\max\limits_{(\xi,\eta)\in\hat{K}} J_K(\xi,\eta)} (A_{PS}^t A_{PS})^{-1} A_B v^5$, then by (42) and (43), we have

$$-\sum_{i=1}^{N} \int_{\partial K_i^* \cap K} \boldsymbol{\tau_v} \boldsymbol{n} \cdot r_h \boldsymbol{v} \mathrm{d}s = \frac{1}{\max\limits_{(\xi,\eta)\in\hat{K}} J_K} (v^5)^t A_B^t (A_{PS}^t A_{PS})^{-1} D A_B v^5,$$

$$\int_K \tilde{\epsilon}(\boldsymbol{v}) : \boldsymbol{\tau_v} \mathrm{d}x\mathrm{d}y = \frac{1}{\max\limits_{(\xi,\eta)\in\hat{K}} J_K} (v^5)^t A_B^t (A_{PS}^t A_{PS})^{-1} \tilde{D} A_B v^5.$$

Direct calculations yield

$$\begin{aligned}\int_K \boldsymbol{\tau_v} : \boldsymbol{\tau_v} \mathrm{d}x\mathrm{d}y &\le \max_{(\xi,\eta)\in\hat{K}} J_K(\xi,\eta) (\beta_{\boldsymbol{v}})^t A_{PS}^t \tilde{H} A_{PS} \beta_{\boldsymbol{v}} \\ &\le \frac{1}{\max\limits_{(\xi,\eta)\in\hat{K}} J_K} (v^5)^t A_B^t (A_{PS}^t A_{PS})^{-1} \tilde{D} A_B v^5.\end{aligned}$$

Note that $A_{PS}^t A_{PS} = \mathrm{diag}(1,1,1,1+\frac{b_1^2}{a_1^2}+\frac{b_1^4}{a_1^4}, 1+\frac{a_2^2}{b_2^2}+\frac{a_2^4}{b_2^4})$, then the second inequality of (50) holds.

For the first inequality in (50), some calculations show

$$\begin{aligned}\int_K \boldsymbol{\tau_v} : \boldsymbol{\tau_v} \mathrm{d}x\mathrm{d}y &\ge \min_{(\xi,\eta)\in\hat{K}} J_K(\xi,\eta) \beta_{\boldsymbol{v}}^t A_{PS}^t \int_{\hat{K}} \Phi^t \Phi \mathrm{d}\xi\mathrm{d}\eta \; A_{PS} \beta_{\boldsymbol{v}} \\ &= \min_{(\xi,\eta)\in\hat{K}} J_K(\xi,\eta) \beta_{\boldsymbol{v}}^t A_{PS}^t A_{PS} \tilde{D} \beta_{\boldsymbol{v}} \\ &\gtrsim \min_{(\xi,\eta)\in\hat{K}} J_K(\xi,\eta) \beta_{\boldsymbol{v}}^t \beta_{\boldsymbol{v}},\end{aligned}$$

and

$$\begin{aligned}\int_K \tilde{\epsilon}(\boldsymbol{v}) : \tilde{\epsilon}(\boldsymbol{v}) \mathrm{d}x\mathrm{d}y &\le \frac{1}{\min\limits_{(\xi,\eta)\in\hat{K}} J_K(\xi,\eta)} (v^5)^t B^t \int_{\hat{K}} \Phi^t \Phi \mathrm{d}\xi\mathrm{d}\eta \; B v^5 \\ &\lesssim \frac{1}{\min\limits_{(\xi,\eta)\in\hat{K}} J_K(\xi,\eta)} (v^5)^t B^t B v^5 \lesssim \frac{1}{\min\limits_{(\xi,\eta)\in\hat{K}} J_K(\xi,\eta)} h_K^2 (v^5)^t v^5.\end{aligned}$$

By the definition of $\beta_{\boldsymbol{v}}$, we have

$$v^5 = \max_{(\xi,\eta)\in\hat{K}} J_K(\xi,\eta) A_B^{-1} (A_{PS}^t A_{PS}) \beta_{\boldsymbol{v}},$$

and $A_B^{-1} = \frac{1}{|A_B|} A_B^*$, where $|A_B| = \frac{J_0^4}{a_1 b_2^2} \eqsim h_K^5$, and $A_B^*$ is the adjoint matrix of $A_B$ with non-zero elements $O(h_K^4)$. Thus

$$(v^5)^t v^5 \lesssim \frac{\big(\max\limits_{(\xi,\eta)\in\hat{K}} J_K(\xi,\eta)\big)^2}{h_K^2} \beta_{\boldsymbol{v}}^t \beta_{\boldsymbol{v}}.$$

Therefore, from Lemma 2.2 it follows the desirable inequality

$$\int_K \tilde{\epsilon}(\boldsymbol{v}) : \tilde{\epsilon}(\boldsymbol{v}) \mathrm{d}x\mathrm{d}y \lesssim \int_K \boldsymbol{\tau}_{\boldsymbol{v}} : \boldsymbol{\tau}_{\boldsymbol{v}} \mathrm{d}x\mathrm{d}y.$$

□

In summary, by Theorems 4.1, 4.2, 4.4, 4.5, and the theory of mixed methods in [8, 10], we arrive at the following well-posedness result for our new method (26)-(27).

**Theorem 4.6.** *Let the partition $\mathcal{T}_h$ satisfy the shape regular condition (5) and the condition (C). Then there exists a unique solution $(\boldsymbol{\sigma}_h, \boldsymbol{u}_h) \in \Sigma_h \times V_h$ for the weak problem (26)-(27) such that*

$$\|\boldsymbol{\sigma}_h\| + |\boldsymbol{u}_h|_1 \lesssim \|\boldsymbol{f}\|.$$

**4.4. ECQ4 element.** In this subsection, we will use a perturbation argument to prove similar stability results for ECQ4 stress mode. We first introduce a well known perturbation result, which can be found in classic books of linear functional analysis.

**Lemma 4.7.** *Let $\mathcal{L}$ be a linear operator between Banach spaces. Suppose $\mathcal{L}^{-1}$ exists and $\|\mathcal{L}^{-1}\| \leq C$. Then for any operator $\boldsymbol{\delta}$ with $\|\boldsymbol{\delta}\| < \frac{1}{C}$, $\mathcal{L} + \boldsymbol{\delta}$ is invertible and*

$$\|(\mathcal{L} + \boldsymbol{\delta})^{-1}\| \leq \frac{C}{1 - \|\mathcal{L}^{-1}\boldsymbol{\delta}\|}.$$

Now let $\mathcal{L}_{PS} = \begin{pmatrix} \mathcal{A} & \tilde{\mathcal{B}} \\ \mathcal{C} & \mathbf{0} \end{pmatrix}$, then by (46) and (47), we see that the operator for ECQ4 is $\mathcal{L}_{EC} = \mathcal{L}_{PS} + \boldsymbol{\delta}_{EC}$, where $\boldsymbol{\delta}_{EC}$ is a high order term under condition (A). The following theorem follows from Lemma 4.7.

**Theorem 4.8.** *Let the partition $\mathcal{T}_h$ satisfy the shape regular condition (5) and the condition (A) and (C). Then, for sufficiently small $h$, $\mathcal{L}_{EC}$ is invertible and $\mathcal{L}_{EC}^{-1}$ is uniformly stable. Namely there exists a unique solution $(\boldsymbol{\sigma}_h, \boldsymbol{u}_h) \in \Sigma_h \times V_h$ for the weak problem (26)-(27) such that*

$$\|\boldsymbol{\sigma}_h\| + |\boldsymbol{u}_h|_1 \lesssim \|\boldsymbol{f}\|.$$

## 5. Uniform a priori error estimates

This section is to derive uniform priori error estimates for our hybrid stress FVM. In addition to the stability conditions established in the previous section, some approximation and consistency results of finite element spaces are required. We first present an approximation result for the affine space

$$Z(\boldsymbol{f}) = \{\boldsymbol{\tau} \in \Sigma_h : \, c(\boldsymbol{v}, \boldsymbol{\tau}) = (\boldsymbol{f}, r_h \boldsymbol{v}) \text{ for all } \boldsymbol{v} \in V_h\}.$$

**Lemma 5.1.** *Let $(\boldsymbol{\sigma}, \boldsymbol{u}) \in H^1(\Omega; \mathbb{R}^{2\times 2}_{sym}) \times (H_0^1(\Omega) \cap H^2(\Omega))^2$ be the weak solution of the problem (2). Under the same conditions as in Theorem 4.5, it holds*

$$\inf_{\theta \in Z(\boldsymbol{f})} \|\boldsymbol{\sigma} - \theta\| \lesssim \inf_{\boldsymbol{\tau} \in \Sigma_h} \sum_{K \in \mathcal{T}_h} (\|\boldsymbol{\sigma} - \boldsymbol{\tau}\|_{0,K} + h_K |\boldsymbol{\sigma} - \boldsymbol{\tau}|_{1,K}) \lesssim h \|\boldsymbol{\sigma}\|_1. \tag{51}$$

*Here $H^1(\Omega; \mathbb{R}^{2\times 2}_{sym})$ denotes $H^1-$integrable symmetric tensor space.*

*Proof.* For any $\boldsymbol{\tau} \in \Sigma_h$, there exists $\zeta \in \Sigma_h$ ( [10], Chapter II, Proposition 1.2), such that

$$c(\boldsymbol{v}, \zeta) = c(\boldsymbol{v}, \boldsymbol{\tau}) - (\boldsymbol{f}, r_h \boldsymbol{v}) \qquad \text{for all } \boldsymbol{v} \in V_h,$$

and

$$\|\zeta\| \lesssim \sup_{\boldsymbol{v} \in V_h} \frac{c(\boldsymbol{v}, \zeta)}{|\boldsymbol{v}|_1}.$$

It is easy to see $\theta = \boldsymbol{\tau} - \zeta \in Z(\boldsymbol{f})$, and

$$\|\boldsymbol{\sigma} - \theta\| \leq \|\boldsymbol{\sigma} - \boldsymbol{\tau}\| + \|\zeta\|.$$

For any $\boldsymbol{v} \in V_h$,

$$\begin{aligned} c(\boldsymbol{v}, \zeta) = c(\boldsymbol{v}, \boldsymbol{\tau}) - (\boldsymbol{f}, r_h \boldsymbol{v}) &= c(\boldsymbol{v}, \boldsymbol{\tau}) - \sum_{i=1}^{N} \int_{K_i^*} -\mathrm{div}\boldsymbol{\sigma} \cdot r_h \boldsymbol{v} \mathrm{d}x\mathrm{d}y \\ &= -\sum_{K \in \mathcal{T}_h} \sum_{i=1}^{N} \int_{\partial K_i^* \cap K} (\boldsymbol{\tau} - \boldsymbol{\sigma}) \boldsymbol{n} \cdot (r_h \boldsymbol{v} - \boldsymbol{v}) \mathrm{d}s \\ &\lesssim \left( \sum_{K \in \mathcal{T}_h} \|\boldsymbol{\sigma} - \boldsymbol{\tau}\|_{0,K}^2 + h_K^2 |\boldsymbol{\sigma} - \boldsymbol{\tau}|_{1,K}^2 \right)^{1/2} |\boldsymbol{v}|_1 \end{aligned}$$

Then

$$\|\boldsymbol{\sigma} - \theta\| \leq \|\boldsymbol{\sigma} - \boldsymbol{\tau}\| + \|\zeta\| \lesssim \sum_{K \in \mathcal{T}_h} \left( \|\boldsymbol{\sigma} - \boldsymbol{\tau}\|_{0,K} + h_K |\boldsymbol{\sigma} - \boldsymbol{\tau}|_{1,K} \right).$$

For any $K \in \mathcal{T}_h$, let $Q_K \boldsymbol{\sigma} = \frac{1}{|K|} \int_K \boldsymbol{\sigma} \mathrm{d}x\mathrm{d}y$. Choosing $\boldsymbol{\tau} = \sum_{K \in \mathcal{T}_h} \chi_K Q_K \boldsymbol{\sigma} \in \Sigma_h$, we get

$$\|\boldsymbol{\sigma} - \theta\| \lesssim \sum_{K \in \mathcal{T}_h} \left( \|\boldsymbol{\sigma} - \boldsymbol{\tau}\|_{0,K} + h_K |\boldsymbol{\sigma} - \boldsymbol{\tau}|_{1,K} \right) \lesssim h \|\boldsymbol{\sigma}\|_1.$$

□

We then present a consistency error estimate.

**Lemma 5.2.** *Let $\pi_h : H^2(\Omega)^2 \to V_h$ be the isoparametric bilinear interpolation operator. Under Condition (B), it holds*

$$\|\tilde{\epsilon}(\pi_h \boldsymbol{v}) - \epsilon(\pi_h \boldsymbol{v})\| \lesssim h \|\boldsymbol{v}\|_2 \qquad \textit{for all } \boldsymbol{v} \in H^2(\Omega)^2. \tag{52}$$

*Proof.* For any element $K \in \mathcal{T}_h$, by scaling technique and interpolation theory, we have

$$\begin{aligned} \|\tilde{\epsilon}(\pi_h \boldsymbol{v}) - \epsilon(\pi_h \boldsymbol{v})\|_{0,K}^2 &\lesssim \frac{\max\{a_{12}^2, b_{12}^2\}}{\min\limits_{(\xi,\eta) \in \hat{K}} J_K(\xi, \eta)} |\hat{\pi}_h \hat{\boldsymbol{v}}|_{1,\hat{K}}^2 \lesssim \frac{\max\{a_{12}^2, b_{12}^2\}}{\min\limits_{(\xi,\eta) \in \hat{K}} J_K(\xi, \eta)} \left( |\hat{\boldsymbol{v}}|_{1,\hat{K}}^2 + |\hat{\boldsymbol{v}}|_{2,\hat{K}}^2 \right) \\ &\lesssim \frac{\max\{a_{12}^2, b_{12}^2\}}{\min\limits_{(\xi,\eta) \in \hat{K}} J_K(\xi, \eta)} \left( |\boldsymbol{v}|_{1,K}^2 + h_K^2 |\boldsymbol{v}|_{2,K}^2 \right). \end{aligned}$$

The result (52) then follows from the assumption that $d_K = O(h_K^2)$. □

We are in the position to state our *a priori* error estimates.

**Theorem 5.3.** *Let $(\boldsymbol{\sigma},\boldsymbol{u})\in H^1(\Omega;\mathbb{R}^{2\times 2}_{sym})\times(H^1_0(\Omega)\cap H^2(\Omega))^2$ be the weak solution of the problem (2). Assume the partition $\mathcal{T}_h$ satisfy the shape regular condition (5) and the condition (B) and (C). Then the problem (26)-(27) admits a unique solution $(\boldsymbol{\sigma}_h,\boldsymbol{u}_h)\in\Sigma_h\times V_h$ such that*

$$\|\boldsymbol{\sigma}-\boldsymbol{\sigma}_h\|+|\boldsymbol{u}-\boldsymbol{u}_h|_1\lesssim h(\|\boldsymbol{\sigma}\|_1+\|\boldsymbol{u}\|_2). \tag{53}$$

*Proof.* For any $\boldsymbol{\theta}\in Z(\boldsymbol{f})$ and $\boldsymbol{v}\in V_h$, since $\boldsymbol{\sigma}_h-\boldsymbol{\theta}\in\ker(\mathcal{C})$, by (29), it holds

$$\begin{aligned}\|\boldsymbol{\sigma}_h-\boldsymbol{\theta}\|&\lesssim\sup_{\boldsymbol{\tau}\in\ker(\tilde{\mathcal{B}})}\frac{a(\boldsymbol{\sigma}_h-\boldsymbol{\theta},\boldsymbol{\tau})}{\|\boldsymbol{\tau}\|}=\sup_{\boldsymbol{\tau}\in\ker(\tilde{\mathcal{B}})}\frac{a(\boldsymbol{\sigma}_h-\boldsymbol{\sigma},\boldsymbol{\tau})+a(\boldsymbol{\sigma}-\boldsymbol{\theta},\boldsymbol{\tau})}{\|\boldsymbol{\tau}\|}\\&\lesssim\sup_{\boldsymbol{\tau}\in\ker(\tilde{\mathcal{B}})}\frac{\tilde{b}(\boldsymbol{u}_h,\boldsymbol{\tau})-b(\boldsymbol{u},\boldsymbol{\tau})}{\|\boldsymbol{\tau}\|}+\|\boldsymbol{\sigma}-\boldsymbol{\theta}\|=\sup_{\boldsymbol{\tau}\in\ker(\tilde{\mathcal{B}})}\frac{\tilde{b}(\boldsymbol{v},\boldsymbol{\tau})-b(\boldsymbol{u},\boldsymbol{\tau})}{\|\boldsymbol{\tau}\|}+\|\boldsymbol{\sigma}-\boldsymbol{\theta}\|\\&\lesssim|\boldsymbol{u}-\boldsymbol{v}|_1+\|\tilde{\epsilon}(\boldsymbol{v})-\epsilon(\boldsymbol{v})\|+\|\boldsymbol{\sigma}-\boldsymbol{\theta}\|.\end{aligned}$$

Using the triangle inequality and Lemma 5.1 and 5.2 and taking $\boldsymbol{v}=\pi_h\boldsymbol{u}$ in the above inequality, we get

$$\|\boldsymbol{\sigma}-\boldsymbol{\sigma}_h\|\lesssim\inf_{\boldsymbol{\theta}\in Z(\boldsymbol{f})}\|\boldsymbol{\sigma}-\boldsymbol{\theta}\|+|\boldsymbol{u}-\pi_h\boldsymbol{u}|_1+\|\tilde{\epsilon}(\pi_h\boldsymbol{u})-\epsilon(\pi_h\boldsymbol{u})\|\lesssim h(\|\boldsymbol{\sigma}\|_1+\|\boldsymbol{u}\|_2).$$

We estimate the approximation of the displacement as follows. For any $\boldsymbol{v}\in V_h$, by the inf-sup condition (34), we have

$$\begin{aligned}|\boldsymbol{u}_h-\boldsymbol{v}|_1&\lesssim\sup_{\boldsymbol{\tau}\in\Sigma_h}\frac{\tilde{b}(\boldsymbol{u}_h-\boldsymbol{v},\boldsymbol{\tau})}{\|\boldsymbol{\tau}\|}=\sup_{\boldsymbol{\tau}\in\Sigma_h}\frac{\tilde{b}(\boldsymbol{u}_h,\boldsymbol{\tau})-b(\boldsymbol{u},\boldsymbol{\tau})+b(\boldsymbol{u},\boldsymbol{\tau})-\tilde{b}(\boldsymbol{v},\boldsymbol{\tau})}{\|\boldsymbol{\tau}\|}\\&\lesssim\sup_{\boldsymbol{\tau}\in\Sigma_h}\frac{\tilde{b}(\boldsymbol{u}_h,\boldsymbol{\tau})-b(\boldsymbol{u},\boldsymbol{\tau})}{\|\boldsymbol{\tau}\|}+|\boldsymbol{u}-\boldsymbol{v}|_1+\|\tilde{\epsilon}(\boldsymbol{v})-\epsilon(\boldsymbol{v})\|\\&=\sup_{\boldsymbol{\tau}\in\Sigma_h}\frac{a(\boldsymbol{\sigma}_h-\boldsymbol{\sigma},\boldsymbol{\tau})}{\|\boldsymbol{\tau}\|}+|\boldsymbol{u}-\boldsymbol{v}|_1\\&\lesssim\|\boldsymbol{\sigma}-\boldsymbol{\sigma}_h\|+|\boldsymbol{u}-\boldsymbol{v}|_1+\|\tilde{\epsilon}(\boldsymbol{v})-\epsilon(\boldsymbol{v})\|.\end{aligned}$$

Again using the triangle inequality and taking $\boldsymbol{v}=\pi_h\boldsymbol{u}$, we obtain

$$|\boldsymbol{u}-\boldsymbol{u}_h|_1\lesssim|\boldsymbol{u}-\pi_h\boldsymbol{u}|_1+\|\tilde{\epsilon}(\pi_h\boldsymbol{u})-\epsilon(\pi_h\boldsymbol{u})\|+\|\boldsymbol{\sigma}-\boldsymbol{\sigma}_h\|\lesssim h(\|\boldsymbol{\sigma}\|_1+\|\boldsymbol{u}\|_2).$$

□

**Remark 5.4.** If we consider the original hybrid stress FV scheme (22)-(23), the results of Theorem 5.3 still hold with Condition (B) being eliminated for PS stress mode or being weakened to Condition (A) for ECQ4 stress mode.

## 6. Numerical experiments

We present some numerical results on several benchmark problems in this section to verify our theoretic results. We refer to [52] for similar examples using hybrid stress FEM. We use $4\times 4$ Gaussian quadrature in all the examples to compute stiffness matrixes and errors. Notice that $2\times 2$ Gaussian quadrature is accurate for computing the stiffness matrix of hybrid stress FVM.

We classify our examples into two categories: plane stress tests and plane strain tests. For each example, we test on both regular meshes, i.e., uniform rectangular meshes, and irregular meshes. Notice that on rectangular meshes the stress modes of PS and ECQ4 are identical. In the plane stress tests, we set $\nu = 0.25$ and $E = 1500$. In the plane strain tests, we set $E = 1500$ and let $\nu \to 0.5$. We list numerical results of $e_{\boldsymbol{\sigma}} = \|\boldsymbol{\sigma} - \boldsymbol{\sigma}_h\|/\|\boldsymbol{\sigma}\|$ for the stress error, and of $e_{\boldsymbol{u}} = |\boldsymbol{u} - \boldsymbol{u}_h|_1/|\boldsymbol{u}|_1$ for the displacement error. We start with two initial meshes shown in Fig 3 and 4 and obtain a sequence of meshes by bisection scheme, i.e. connect the midpoints of the opposite edges.

**6.1. Plane stress tests.** We will use two plane stress beam models to test our new FVM method.

**Example 6.1** (Plane stress test 1)**.** *A plane stress beam modeled with rectangular domain is tested, where the origin of the coordinates $x$, $y$ is at the midpoint of the left end, the body force $\boldsymbol{f} = (0,\, 0)^t$, the surface traction $\boldsymbol{g}$ on $\Gamma_N = \{(x, y) \in [0, 10] \times [-1, 1] : x = 10$ or $y = \pm 1\}$ given by $\boldsymbol{g}|_{x=10} = (-2Ey, 0)^t$, $\boldsymbol{g}|_{y=\pm 1} = (0, 0)^t$, and the exact solution is given by*

$$\boldsymbol{u} = \begin{pmatrix} -2xy \\ x^2 + \nu(y^2 - 1) \end{pmatrix},\ \boldsymbol{\sigma} = \begin{pmatrix} -2Ey & 0 \\ 0 & 0 \end{pmatrix}.$$

*The numerical results are listed in Table 1.*

**Example 6.2** (Plane stress test 2)**.** *The body force $\boldsymbol{f} = -(6y^2,\, 6x^2)^t$, the surface traction $\boldsymbol{g}$ on $\Gamma_N = \{(x, y) : x = 10,\ -1 \le y \le 1\}$ is $\boldsymbol{g} = (0,\, 2000 + 2y^3)^t$, and the exact solution is given by*

$$\boldsymbol{u} = \frac{1+\nu}{E}(y^4,\, x^4)^t,\ \boldsymbol{\sigma} = \begin{pmatrix} 0 & 2(x^3 + y^3) \\ 2(x^3 + y^3) & 0 \end{pmatrix}.$$

*The numerical results are listed in Table 2.*

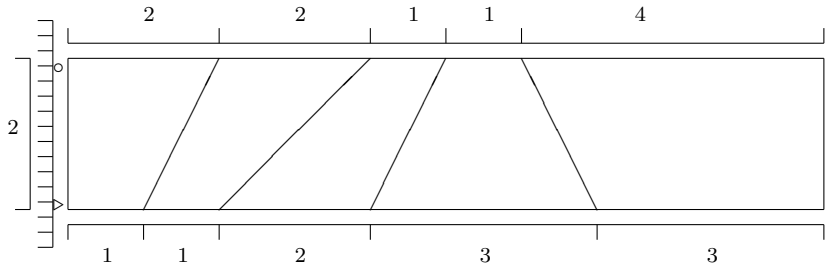


FIGURE 3. Domain of Example 6.1-6.4 and the partition of the $5 \times 1$ irregular mesh.

**6.2. Plane strain tests.** We will use two plane strain pure bending cantilever beams to test our hybrid stress FVM method.

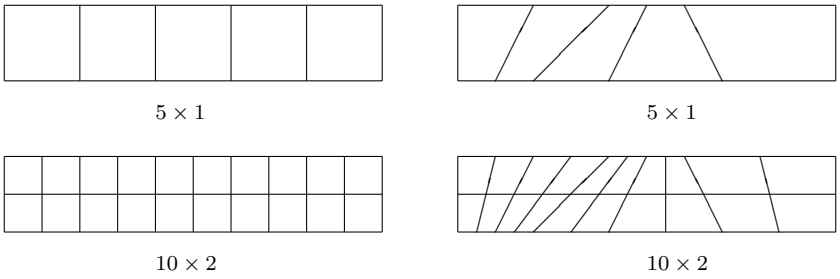


FIGURE 4. Regular and irregular meshes

TABLE 1. The results of $e_{\boldsymbol{u}}$ and $e_{\boldsymbol{\sigma}}$ for the new FVM in Example 6.1.

| | | $10\times 2$ | $20\times 4$ | $40\times 8$ | $80\times 16$ | $160\times 32$ |
|---|---|---|---|---|---|---|
| Regular mesh | $e_{\boldsymbol{u}}$ | 0.0363 | 0.0182 | 0.0091 | 0.0045 | 0.0023 |
| | $e_{\boldsymbol{\sigma}}$ | 0 | 0 | 0 | 0 | 0 |
| PS: | $e_{\boldsymbol{u}}$ | 0.4510 | 0.2208 | 0.0738 | 0.0212 | 0.0064 |
| Irregular mesh | $e_{\boldsymbol{\sigma}}$ | 0.5601 | 0.3591 | 0.1952 | 0.0998 | 0.0502 |
| ECQ4: | $e_{\boldsymbol{u}}$ | 0.4551 | 0.2214 | 0.0737 | 0.0212 | 0.0064 |
| Irregular mesh | $e_{\boldsymbol{\sigma}}$ | 0.5644 | 0.3604 | 0.1954 | 0.0998 | 0.0502 |

TABLE 2. The results of $e_{\boldsymbol{u}}$ and $e_{\boldsymbol{\sigma}}$ for the new FVM in Example 6.2.

| | | $10\times 2$ | $20\times 4$ | $40\times 8$ | $80\times 16$ | $160\times 32$ |
|---|---|---|---|---|---|---|
| Regular meshes | $e_{\boldsymbol{u}}$ | 0.01096 | 0.0583 | 0.0299 | 0.0151 | 0.0076 |
| | $e_{\boldsymbol{\sigma}}$ | 0.0904 | 0.0489 | 0.0251 | 0.0127 | 0.0063 |
| PS: | $e_{\boldsymbol{u}}$ | 0.1882 | 0.0990 | 0.0516 | 0.0263 | 0.0132 |
| Irregular meshes | $e_{\boldsymbol{\sigma}}$ | 0.1874 | 0.0982 | 0.0506 | 0.0256 | 0.0129 |
| ECQ4: | $e_{\boldsymbol{u}}$ | 0.1886 | 0.0992 | 0.0517 | 0.0263 | 0.0132 |
| Irregular meshes | $e_{\boldsymbol{\sigma}}$ | 0.2020 | 0.1063 | 0.0546 | 0.0276 | 0.0138 |

TABLE 3. The results of $e_{\boldsymbol{u}}$ and $e_{\boldsymbol{\sigma}}$ for the new FVM in Example 6.3: regular meshes

| $\nu$ | | $5\times 1$ | $10\times 2$ | $20\times 4$ | $40\times 8$ |
|---|---|---|---|---|---|
| 0.499 | $e_{\boldsymbol{u}}$ | 0.0993 | 0.0497 | 0.0248 | 0.0124 |
| | $e_{\boldsymbol{\sigma}}$ | 0 | 0 | 0 | 0 |
| 0.4999 | $e_{\boldsymbol{u}}$ | 0.0995 | 0.0497 | 0.0249 | 0.0124 |
| | $e_{\boldsymbol{\sigma}}$ | 0 | 0 | 0 | 0 |
| 0.49999 | $e_{\boldsymbol{u}}$ | 0.0995 | 0.0497 | 0.0249 | 0.0124 |
| | $e_{\boldsymbol{\sigma}}$ | 0 | 0 | 0 | 0 |

**Example 6.3** (Plane strain test 1)**.** *A plane strain pure bending cantilever beam on rectangular domain* $\Omega = \{(x, y) : 0 < x < 10, -1 < y < 1\}$ *is used to test locking-free performance. The body force* $\boldsymbol{f} = (0, 0)^t$*, the surface traction* $\boldsymbol{g}$ *on* $\Gamma_N = \{(x, y) \in$

TABLE 4. The results of $e_{\boldsymbol{u}}$ and $e_{\boldsymbol{\sigma}}$ for the new FVM based on PS stress in Example 6.3: irregular mesh.

| $\nu$ | | $10\times 2$ | $20\times 4$ | $40\times 8$ | $80\times 16$ | $160\times 32$ |
|---|---|---|---|---|---|---|
| 0.499 | $e_{\boldsymbol{u}}$ | 0.4438 | 0.2159 | 0.0726 | 0.0213 | 0.0067 |
| | $e_{\boldsymbol{\sigma}}$ | 0.5879 | 0.3650 | 0.1959 | 0.0999 | 0.0502 |
| 0.4999 | $e_{\boldsymbol{u}}$ | 0.4438 | 0.2158 | 0.0726 | 0.0213 | 0.0068 |
| | $e_{\boldsymbol{\sigma}}$ | 0.5882 | 0.3650 | 0.1959 | 0.0999 | 0.0502 |
| 0.49999 | $e_{\boldsymbol{u}}$ | 0.4438 | 0.2158 | 0.0726 | 0.0213 | 0.0068 |
| | $e_{\boldsymbol{\sigma}}$ | 0.5883 | 0.3650 | 0.1959 | 0.0999 | 0.0502 |

TABLE 5. The results of $e_{\boldsymbol{u}}$ and $e_{\boldsymbol{\sigma}}$ for the new FVM based on ECQ4 stress in Example 6.3: irregular meshes.

| $\nu$ | | $10\times 2$ | $20\times 4$ | $40\times 8$ | $80\times 16$ | $160\times 32$ |
|---|---|---|---|---|---|---|
| 0.499 | $e_{\boldsymbol{u}}$ | 0.4492 | 0.2169 | 0.0727 | 0.0213 | 0.0067 |
| | $e_{\boldsymbol{\sigma}}$ | 0.5909 | 0.3660 | 0.1961 | 0.0999 | 0.0502 |
| 0.4999 | $e_{\boldsymbol{u}}$ | 0.4492 | 0.2169 | 0.0727 | 0.0213 | 0.0068 |
| | $e_{\boldsymbol{\sigma}}$ | 0.5911 | 0.3660 | 0.1961 | 0.0999 | 0.0502 |
| 0.49999 | $e_{\boldsymbol{u}}$ | 0.4491 | 0.2169 | 0.0727 | 0.0213 | 0.0068 |
| | $e_{\boldsymbol{\sigma}}$ | 0.5912 | 0.3660 | 0.1961 | 0.0999 | 0.0502 |

TABLE 6. The results of $e_{\boldsymbol{u}}$ and $e_{\boldsymbol{\sigma}}$ for the new FVM in Example 6.4: regular meshes.

| $\nu$ | | $10\times 2$ | $20\times 4$ | $40\times 8$ | $80\times 16$ | $160\times 32$ |
|---|---|---|---|---|---|---|
| 0.499 | $e_{\boldsymbol{u}}$ | 0.1023 | 0.0544 | 0.0282 | 0.0143 | 0.0072 |
| | $e_{\boldsymbol{\sigma}}$ | 0.2390 | 0.0680 | 0.0291 | 0.0140 | 0.0069 |
| 0.4999 | $e_{\boldsymbol{u}}$ | 0.1022 | 0.0544 | 0.0282 | 0.0143 | 0.0072 |
| | $e_{\boldsymbol{\sigma}}$ | 0.3514 | 0.0920 | 0.0316 | 0.0142 | 0.0069 |
| 0.49999 | $e_{\boldsymbol{u}}$ | 0.1022 | 0.0544 | 0.0282 | 0.0143 | 0.0072 |
| | $e_{\boldsymbol{\sigma}}$ | 0.3748 | 0.1045 | 0.0360 | 0.0150 | 0.0070 |

$[0,10]\times[-1,1]:\ x=10$ *or* $y=\pm 1\}$ *given by* $\boldsymbol{g}|_{x=10}=(-2Ey,0)^t$, $\boldsymbol{g}|_{y=\pm 1}=(0,0)^t$, *and the exact solution reads as*

$$\boldsymbol{u}=\begin{pmatrix} -2(1-\nu^2)xy \\ (1-\nu^2)x^2+\nu(1+\nu)(y^2-1)\end{pmatrix},\ \boldsymbol{\sigma}=\begin{pmatrix} -2Ey & 0\\ 0 & 0\end{pmatrix}.$$

*The numerical results are listed in Tables 3-5.*

**Example 6.4** (Plane strain test 2)**.** *The body force* $\boldsymbol{f}=-(6y^2,\,6x^2)^t$, *the surface traction* $\boldsymbol{g}$ *on* $\Gamma_N=\{(x,y):\ x=10,\ -1\le y\le 1\}$ *is given by* $\boldsymbol{g}=(0,\,2000+2y^3)^t$, *and the exact solution reads as*

$$\boldsymbol{u}=\frac{1+\nu}{E}(y^4,\,x^4)^t,\ \boldsymbol{\sigma}=\begin{pmatrix} 0 & 2(x^3+y^3)\\ 2(x^3+y^3) & 0\end{pmatrix}.$$

*The numerical results are listed in Tables 6-8.*

From Tables 1-8, we have the following observations.

TABLE 7. The results of $e_{\boldsymbol{u}}$ and $e_{\boldsymbol{\sigma}}$ for the new FVM based on PS stress in Example 6.4: irregular meshes.

| $\nu$ | | $10\times 2$ | $20\times 4$ | $40\times 8$ | $80\times 16$ | $160\times 32$ |
|---|---|---|---|---|---|---|
| 0.499 | $e_{\boldsymbol{u}}$ | 0.1967 | 0.0954 | 0.0490 | 0.0249 | 0.0126 |
| | $e_{\boldsymbol{\sigma}}$ | 0.4921 | 0.1491 | 0.0663 | 0.0322 | 0.0160 |
| 0.4999 | $e_{\boldsymbol{u}}$ | 0.1970 | 0.0954 | 0.0490 | 0.0249 | 0.0126 |
| | $e_{\boldsymbol{\sigma}}$ | 0.8380 | 0.1884 | 0.0697 | 0.0326 | 0.0160 |
| 0.49999 | $e_{\boldsymbol{u}}$ | 0.1971 | 0.0953 | 0.0490 | 0.0249 | 0.0126 |
| | $e_{\boldsymbol{\sigma}}$ | 0.9494 | 0.2132 | 0.0751 | 0.0334 | 0.0161 |

TABLE 8. The results of $e_{\boldsymbol{u}}$ and $e_{\boldsymbol{\sigma}}$ for the new FVM based on ECQ4 stress in Example 6.4: irregular meshes.

| $\nu$ | | $10\times 2$ | $20\times 4$ | $40\times 8$ | $80\times 16$ | $160\times 32$ |
|---|---|---|---|---|---|---|
| 0.499 | $e_{\boldsymbol{u}}$ | 0.1871 | 0.0969 | 0.0503 | 0.0256 | 0.0129 |
| | $e_{\boldsymbol{\sigma}}$ | 0.2297 | 0.1185 | 0.0604 | 0.0304 | 0.0152 |
| 0.4999 | $e_{\boldsymbol{u}}$ | 0.1871 | 0.0969 | 0.0503 | 0.0256 | 0.0129 |
| | $e_{\boldsymbol{\sigma}}$ | 0.2298 | 0.1185 | 0.0604 | 0.0304 | 0.0152 |
| 0.49999 | $e_{\boldsymbol{u}}$ | 0.1871 | 0.0969 | 0.0503 | 0.0256 | 0.0129 |
| | $e_{\boldsymbol{\sigma}}$ | 0.2298 | 0.1185 | 0.0604 | 0.0304 | 0.0152 |

(1) Hybrid stress FVM is of first order convergence rate for the displacement and stress approximations in all the plane stress and strain tests.
(2) The method is locking free in the plane strain tests in the sense that it yields uniform results as $\lambda \to \infty$ or Poisson ratio $\nu \to 0.5$. Especially, on coarse meshes the method based on ECQ4 stress mode behaves better than that on PS stress mode; compare the second column of Table 7 and 8.

## 7. Summary and future work

We have proposed for the stress-displacement fields linear elasticity problems a hybrid stress finite volume method which couples a finite volume formulation with a hybrid stress finite element formulation. The method is shown to be uniformly convergent with respect to the Lamé constant $\lambda$. Due to the elimination of stress parameters at the element level, the computational cost of this approach is almost the same as that of the standard bilinear element.

In future work we shall consider *a posteriori* error estimate and the superconvergence recovery for the stress along the line of [55, 38].

## Acknowledgments

The first and second authors were supported by the National Natural Science Foundation of China (11171239). The second author was also supported by the Foundation for Excellent Young Scholars of Sichuan University (2011SCU04B28). The third author was supported by NSF Grant DMS-0811272, DMS-1115961, and in part by 2010-2011 UC Irvine Academic Senate Council on Research, Computing and Libraries (CORCL).

## References


[1] D. N. Arnold, Discretization by finite elements of a model parameter dependent problem, Numer. Math., 37 (1981), pp 405–421.

[2] D. N. Arnold, G. Awanou, and R.Winther, Finite elements for symmetric tensors in three dimensions, Math. Comp., 77 (2008), pp 1229–1251.

[3] D. N. Arnold and R. Winther, Mixed finite elements for elasticity, Numer. Math., 92 (2002), pp 401–419.

[4] G. Awanou, Symmetric Matrix Fields in the Finite Element Method, Symmetry, 2 (2010), PP 1375–1389.

[5] I. Babŭska and M. Suri, Locking effects in the finite element approximation of elasticity problems, Numer. Math., 62 (1992), PP 439–463.

[6] C. Bailey, M. Cross, A finite volume procedure to solve elastic solid mechanics problems in three dimensions on an unstructured mesh, Int. J. Numer. Meth. Engng., 38 (1995), pp 1757–1776.

[7] R. E. Bank, D. J. Rose, Some error estimates for the box method, SIAM J. Numer. Anal., 24 (1987), pp 351–375.

[8] Christine Bernardi, Claudio Canuto, Yvon Maday, Generalized inf-sup conditions for chebyshev spectral approximation of the Stokes problem, SIAM J. Numer. Anal., 25 (1988), pp 1237–1271.

[9] I. Bijelonja, I. Demirdžić, S. Muzaferija, A finite volume method for incompressible linear elasticity, Comput. Methods Appl. Mech. Engrg., 195 (2006), pp 6378–6390.

[10] Franco Brezzi, Michel Fortin, Mixed and hybrid finite element methods, Springer-Verlag, 1991.

[11] C. Carstensen, Xiaoping Xie, Guozhu Yu, Tianxiao Zhou, A priori and posteriori analysis for a locking-free low order quadrilateral hybrid finite element for Reissner-Mindlin plates, Comput. Methods Appl. Mech. Engrg., 200 (2011), pp 1161-1175.

[12] Long Chen, A new class of high order finite volume methods for second order elliptic equations, SIAM J. Numer. Anal., 47 (2009), pp 4021–4043.

[13] S. H. Chou, D. Y. Kwak, A covolume method based on rotated bilinears for the Generalized Stokes problem, SIAM J. Numer. Anal., 35 (1998), pp 494–507.

[14] S. H. Chou, D. Y. Kwak, A general framework for constructing and analyzing mixed finite volume methods on quadrilateral grids: The overlapping covolume case, SIAM J. Numer. Anal., 39 (2002), pp 1170–1196.

[15] S. H. Chou, D. Y. Kwak, Kwang Y. Kim, Mixed finite volume methods on nonstaggered quadrilateral grids for elliptic problems, Math. Comput., 72 (2002), pp 525–539.

[16] S. Chou and P. Vassilevski, A general mixed covolume framework for constructing conservative schemes for elliptic problems, Math. Comp., 69 (1999), pp 991–1012.

[17] I. Demirdi and S. Muzaferija, Numerical method for coupled fluid flow, heat transfer and stress analysis using unstructured moving meshes with cells of arbitrary topology, Comput. Methods Appl. Mech. Engrg., 125 (1995), pp 235–255.

[18] N. Fallah, A cell vertex and cell centred finite volume method for plate bending analysis, Comput. Methods Appl. Mech. Engrg., 193 (2004), pp 3457–3470.

[19] N. Fallah, C. Bailey, M. Cross, and G. Taylor, Comparison of finite element and finite volume methods application in geometrically nonlinear stress analysis, Applied Mathematical Modelling, 24 (2000), pp 439–455.

[20] J. H. Ferziger, Milovan Peric, Computational Methods for Fluid Dynamics, Springer, 1999.

[21] W. Hackbusch., On first and second order box schemes. Computing, 41(1989):277–296.

[22] C. Hirsch, Numerical Computation of Internal and External Flow, Vol. I, Wiley, New York, 1989

[23] Jun Hu, Zhong-Ci Shi, Lower order rectangular nonconforming mixed finite elements for plane elasticity, SIAM J Numer Anal, 46(2007), pp 88–102

[24] H. Jasak and H. G. Weller, Application of the finite volume method and unstructured meshes to linear elasticity, Int. J. Numer. Meth. Engng., 48 (2000), pp 267–287.

[25] Kays W. M., Crawford Michael, Convective heat and mass transfer (4th Ed), New York. 1993.

[26] Yong-hai Li, Rong-hua Li, Generalized difference methods on arbitrary quadrilateral networks, Journal of Computational Mathematics, 17 (1999), pp 653–672.

[27] A. Limachea and S. Idelsohnb, On the development of finite volume methods for computational solid mechanices, Mechanica Computacional, 26 (2007), pp 827–843.

[28] Hong-ying Man, Zhong-ci Shi, $P_1-$nonconforming quadrilateral finite volume element method and its cascadic multigrid algorithm for elliptic problems, Journal of Computational Mathematics, 24 (2006), pp 59–80.

[29] E. Oñate, M. Cervera and C. Zienkiewicz, A finite volume formart for structural mechanics, Int. J. Numer. Meth. Engng., 37 (1994), pp 181–201.

[30] S. V. Patankar, in W. J. Minkowycz and E. M. Sparrow (eds.), Numerical Heat Transfer and Fluid Flow, Series in Computational Methods in Mechanics and Thermal Sciences, Hemisphere, Washington, DC, 1980.

[31] T. H. H. Pian, Derivation of element stiffness matrices by assumed stress distributions, A.I.A.A.J., 2: 1333-1336 (1964).

[32] T. H. H. Pian, K. Sumihara, Rational approach for assumed stress finite element methods, Int. J. Numer. Meth. Engng., 20 (1984), pp 1685–1695.

[33] T. H. H. Pian, D. P. Chen, Alternative ways of for formulation of hybrid stress elements, Int. J. Numer. Meths. Engng., 18: 1679-1684 (1982).

[34] T. H . H. Pian and Pin Tong, Relation between incompatible displacement model and hybrid stress model, Int. J. Numer. Meth Engng., 22: 173-182 (1989).

[35] T. H. H. Pian, C. C. Wu, A rational approach for choosing stress term of hybrid finite element formulations, Int. J. Numer. Meth. Engng., 26: 2331-2343 (1988).

[36] T. H. H. Pian and C. Wu, Hybrid and incompatible finite element methods, CRC Press, 2006.

[37] Zhong-Ci Shi, A convergence condition for the quadrilateral Wilson element, Numer. Math., 44 (1984), pp 349–361.

[38] Zhong-Ci Shi, Xuejun Xu, and Zhimin Zhang, The patch recovery for finite element approximation of elasticity problems under quadrilateral meshes, Discrete and Continuous Dynamical Systems - Series B 9-1 (2008), pp 163–182.

[39] Shi Shu, Haiyuan Yu, Yunqing Huang, Cunyun Nie, A symmetric finite volume element scheme on quadrilateral grids and superconvergence, International Journal of Numerical Analysis and Modeling, 3 (2006), pp 348–360.

[40] A. Slone, C. Bailey, and M. Cross, Dynamic solid mechanics using finite volume methods, Applied mathematical modelling, 27 (2003), pp 69–87.

[41] Souli M., Ouahsine A., Lewin L., Ale formulation for fluid-structure interaction problems, Computer Methods in Applied Mechanics and Engineering, 190 (2000), pp 659-C675.

[42] M. Suri, I. Babuska, and C. Schwab, Locking effects in the finite element approximation of plate models, Math. Comp., 64 (1995), pp 461–482.

[43] G. A. Taylor, C. Bailey, M. Cross, Solution of the elastic/visco-plastic constitutive equations: A finite volume approach, Appl. Math. Modelling, 9 (1995), pp 746–760.

[44] Versteeg H. K., Malalasekera W., An introduction to computational fluid dynamics: The finite volume method, New York (Harlow, Essex, England and Longman Scientific & Technical), 1995.

[45] P. Wapperom, M. Webster, A Second-order Hybrid Finite Element/Volume Method for Viscoelastic Flows, Journal of Non-Newtonian Fluid Mechanics, 79(1998), pp 405–431.

[46] M. A. Wheel, A finite volume method for analysis the bending deformation of thick and thin plates, Comput. Methods Appl. Mech. Engrg., 147 (1997), pp 199–208.

[47] M. L. Wilkins, Calculations of elasto-plastic flow, Methods of Computational Physics, Vol. 3, Academic Press, New York, 1964.

[48] Xiaoping Xie, An accurate hybrid macro-element with linear displacements, Commun. Numer. Meth. Engng., 21:1-12 (2005).

[49] Xiaoping Xie, Jinchao Xu, New mixed finite elements for plane elasticity and Stokes equation, Science China Mathematics, 2011, 54(7): 1499-1519

[50] Xiaoping Xie, Tianxiao Zhou, Optimization of stress modes by energy compatibility for 4-node hybrid quadrilaterals, Int. J. Numer. Meth. Engng, 59 (2004), pp 293–313.

[51] Xiaoping Xie, Tianxiao Zhou, Accurate 4-node quadrilateral elements with a new version of energy-compatible stress mode, Commun. Numer. Meth. Engng., 24:125-139 (2008).

[52] Guozhu Yu, Xiaoping Xie, Carsten Carstense, Uniform convergence and a posterior error estimation for assumed stress hybrid finite element methods, Comput. Methods Appl. Mech. Engrg., 200 (2011), pp 2421-2433.

[53] Shiquan Zhang, Xiaoping Xie, Accurate 8-node hybrid hexahedral elements with energy-compatible stress modes Adv. Appl. Math. Mech., 2010, Vol. 2, No. 3, pp. 333-354.

[54] Zhimin Zhang, Ananlysis of some quadrilateral nonconforming elements for incompressible elasticity, SIAM J. Numer. Anal., 34 (1997), pp 640–663.

[55] Zhimin Zhang, Polynomial preserving gradient recovery and a posteriori estimate for bilinear element on irregular quadrilaterals, International Journal of Numerical Analysis and Modelling 1 (2004), pp 1–24.

[56] Tianxiao Zhou, Xiaoping Xie, A unified analysis for stress/strain hybrid methods of high performance, Comput. Methods Appl. Mech. Engrg., 191 (2002), pp 4619-C4640.

[57] O. C. Zienkiewicz and E. Oñate, Finite elements versus finite volumes. Is there really a choice?, in P. Wriggers and W. Wagner, Nonlinear Computation Mechanics. State of the Art, Springer, Berlin, 1991.

Structure Mechanical Institute, CAEP, Mianyang 621900, China. School of Mathematics, Sichuan University, Chengdu 610064, China.

*E-mail*: wuyongkescu06@yahoo.com.cn

School of Mathematics, Sichuan University, Chengdu 610064, China.

*E-mail*: xpxiec@gmail.com

Department of Mathematics, University of California at Irvine, Irvine, CA 92697

*E-mail*: chenlong@math.uci.edu